Fast and accurate integral equation methods with applications in microfluidics

LUDVIG AF KLINTEBERG

Akademisk avhandling som med tillstånd av Kungl Tekniska högskolan framlägges till offentlig granskning för avläggande av teknologie doktorsexamen i tillämpad matematik och beräkningsmatematik med inriktning mot numerisk analys torsdagen den 2 juni 2016 klockan 10.00 i sal F3, Lindstedtsvägen 26, KTH, Stockholm.

Abstract

This thesis is concerned with computational methods for fluid flows on the microscale, also known as microfluidics. This is motivated by current research in biological physics and miniaturization technology, where there is a need to understand complex flows involving microscale structures. Numerical simulations are an important tool for doing this.

The first, and smaller, part of the thesis presents a numerical method for simulating multiphase flows involving insoluble surfactants and moving contact lines. The method is based on an interface decomposition resulting in local, Eulerian grid representations. This provides a natural setting for solving the PDE governing the surfactant concentration on the interface.

The second, and larger, part of the thesis is concerned with a framework for simulating large systems of rigid particles in three-dimensional, periodic viscous flow using a boundary integral formulation. This framework can solve the underlying flow equations to high accuracy, due to the accurate nature of surface quadrature. It is also fast, due to the natural coupling between boundary integral methods and fast summation methods.

The development of the boundary integral framework spans several different fields of numerical analysis. For fast computations of large systems, a fast Ewald summation method known as Spectral Ewald is adapted to work with the Stokes double layer potential. For accurate numerical integration, a method known as Quadrature by Expansion is developed for this same potential, and also accelerated through a scheme based on geometrical symmetries. To better understand the errors accompanying this quadrature method, an error analysis based on contour integration and calculus of residues is carried out, resulting in highly accurate error estimates.

Sammanfattning

Denna avhandling behandlar beräkningsmetoder för strömning på mikroskalan, även känt som mikrofluidik. Detta val av ämne motiveras av aktuell forskning inom biologisk fysik och miniatyrisering, där det ofta finns ett behov av att förstå komplexa flöden med strukturer på mikroskalan. Datorsimuleringar är ett viktigt verktyg för att öka den förståelsen.

Avhandlingens första, och mindre, del beskriver en numerisk metod för att simulera flerfasflöden med olösliga surfaktanter och rörliga kontaktlinjer. Metoden är baserad på en uppdelning av gränsskiktet, som tillåter det att representeras med lokala, Euleriska nät. Detta skapar naturliga förutsättningar för lösning av den PDE som styr surfaktantkoncentrationen på gränsskiktets yta.

Avhandlingens andra, och större, del beskriver ett ramverk för att med hjälp av en randintegralformulering simulera stora system av styva partiklar i tredimensionellt, periodiskt Stokesflöde. Detta ramverk kan lösa flödesekvationerna mycket noggrant, tack vare den inneboende höga noggrannheten hos metoder för numerisk integration på släta ytor. Metoden är också snabb, tack vare den naturliga kopplingen mellan randintegralmetoder och snabba summeringsmetoder.

Utvecklingen av ramverket för partikelsimuleringar täcker ett brett spektrum av ämnet numerisk analys. För snabba beräkningar på stora system används en snabb Ewaldsummeringsmetod vid namn spektral Ewald. Denna metod har anpassats för att fungera med den randintegralformulering för Stokesflöde som används. För noggrann numerisk integration används en metod kallad expansionskvadratur (eng. Quadrature by Expansion), som också har utvecklats för att passa samma Stokesformulering. Denna metod har även gjorts snabbare genom en nyutvecklad metod baserad på geometriska symmetrier. För att bättre förstå kvadraturmetodens inneboende fel har en analys baserad på konturintegraler och residykalkyl utförts, vilket har resulterat i väldigt noggranna felestimat.

Preface

This is a compilation thesis divided into two parts. Part I consists of the introductory chapters, which introduce the subject and summarize the thesis work. Part II consists of the included papers, which are four full length papers (I–IV) and a short note (paper V).

- Paper I presents an extension of previous work by DL and AKT. LK contributed to the ideas, methods and their implementations, performed the numerical computations and wrote a portion of the manuscript.

- Papers II-IV present work carried out in collaboration with AKT. LK contributed to the ideas and methods, implemented the methods, performed the numerical computations and wrote the manuscripts.

- Paper V is a short note containing results that were needed in Paper IV, but were considered out of scope. LK derived the results and wrote the note.

The included papers are:

Paper I

L. af Klinteberg, D. Lindbo, and A.-K. Tornberg. An explicit Eulerian method for multiphase flow with contact line dynamics and insoluble surfactant. *Computers & Fluids*, vol. 101, pp. 50–63, 2014.

Paper II

L. af Klinteberg and A.-K. Tornberg. Fast Ewald summation for Stokesian particle suspensions. *International Journal for Numerical Methods in Fluids*, vol. 76, no. 10, pp. 669–698, 2014.

Paper III

L. af Klinteberg and A.-K. Tornberg. Estimation of quadrature errors in layer potential evaluation using quadrature by expansion. *Preprint, arXiv:1603.08366 [math.NA]*, 2016.

Paper IV

L. af Klinteberg and A.-K. Tornberg. A fast integral equation method for solid particles in viscous flow using quadrature by expansion. *Preprint, arXiv:1604.07186 [math.NA]*, 2016.

Paper V

L. af Klinteberg. Ewald summation for the rotlet singularity of Stokes flow. *Technical note, arXiv:1603.07467 [physics.flu-dyn]*, 2016.

Acknowledgments

First of all I want to thank my advisor Anna-Karin Tornberg for your trust in me. When you took me in I was a young, slightly overconfident student with a mathematical background that could have been stronger. Over the years you have given me the freedom to find my own solutions, while always being available for discussions. Now, almost seven (!) years later, I feel that I am finally beginning to understand a thing or two, and I would not have been here without your guidance and inspiration.

Over the years I have shared offices with Jeanette, Rodrigo, Dag, Niclas, Jelena, Jennifer, Gohar, a Moccamaster, and a brown sofa — many of whom I now count among my friends. Together we've had long whiteboard sessions, huge amounts of coffee, countless discussions about math and programming, too much "Asian wok", and a very, very good time. Outside of my office I have been fortunate enough to be surrounded by great colleagues, both at NADA and Mathematics, and many good discussions have sprung out of small talk by the office coffee machine. Thank you all.

I would also like to thank Ericsson Systems & Technology for giving me the opportunity to do an internship there, in spite of my nonexistent experience with telecommunication. And thank you Dag for making it happen.

Finally, I want to thank my family. Thank you Elin for being by my side all the way, even though I sometimes forget about everything outside my own head. You have a greater part in this than you think. And thank you Lilly and Hilda for dragging me back to reality whenever my attention wanders. You help me get perspective.

Ludvig af Klinteberg
Stockholm, April 2016

Contents

Chapter 1

Introduction

Fluids — meaning gases and liquids — are a central part of the world we live in, and the subject of fluid mechanics studies how fluids behave in different situations. The wind and rain outside the window, the air we breathe and the blood flowing in our veins are all governed by the same physical laws. These laws are well described by Navier-Stokes equations for incompressible flow of Newtonian fluids (stated on page 6), which describe almost all of the fluid phenomena we see around us[1]. This set of partial differential equations (PDEs) is nonlinear and very challenging to work with. Real world problems, such as the question of how the air flows around (and lifts!) and airplane or how the water flows around a ship hull, can not be solved by purely theoretical considerations. Before the advent of computers, engineers and scientists had to rely solely on experimental work in wind tunnels and towing tanks if they wanted to analyze these flows. In the 1960's the first computer simulations of fluid flows were performed, and the last half-century has seen a massive development of both computer power and numerical methods. Today we can play computer games with real-time smoke effects, and we regularly expect the weather simulations of our meteorological institutes to predict the flow patterns of the sky more than a week into the future. Scientists and engineers are now abandoning their wind tunnels in favor of computer simulations, which offer cheap and accurate results without even having to get your hands dirty.

1.1   Microfluidics

The field of microfluidics deals with fluid flows at the micrometer scale. It has grown continuously since the 1990's, motivated by questions arising from biological physics and advances in miniaturization technology, especially in what is referred to as lab-on-a-chip devices (see for example Tabeling [94] and Stone [92] for a thorough introduction to the subject). The idea of these devices is to take all the steps of a

---

[1]Some flows require the general form of the Navier-Stokes equations, for example ketchup flow (non-Newtonian liquid) and the airflow around a supersonic fighter jet (compressible flow).

certain laboratory process, miniaturize them and put them together on one chip. A typical blood sample analysis, where one wants to detect whether a certain protein or hormone is present in a patient's blood, can for example be miniaturized, thereby reducing the required sample volume to a nano- or picoliter, and at the same time speeding up the analysis time. One could potentially construct a device which splits a single drop of blood into a thousand small droplets and performs a different analysis on each droplet, giving a doctor an immediate overview of a patients health.

At the small length scales considered in microfluidics, effects related to fluid viscosity — like the upstream buckling we observe when pouring syrup on pancakes — start to dominate over the inertial effects that we are used to observing around us — like the chaotic sloshing which we associate with trying to walk quickly while carrying a mug full of coffee. At the same time, effects related to surfaces and fluid interfaces become more pronounced as the surface-to-volume ratio increases. As an example, consider a box with sides L, filled with a liquid. The surface-to-volume ratio of such a box is 6:L. In the case of the box being a large tank with side $L = 6$ m the ratio would be 1:1, while in the case of the box being a miniature container with side one micrometer, $L = 10^{-6}$ m, the ratio would be 6000000:1. From this one can understand that flow effects related to physics happening at the surfaces of the box would have a much larger relative importance in the miniature case. As these surface effects become increasingly important when we scale down our problems, so does the need to accurately model and capture them in numerical simulations.

1.2   Overview of this thesis

In chapter 2 of this thesis we discuss a method for accurately simulating multiphase flows, which are fluid flows containing interfaces between gases and liquids, such as drops and bubbles, or between immiscible liquids, such as oil and water. We show how the method can be used to handle flow problems where there are surface tension altering chemicals present on the surface, and further extend it to handle wetting problems, where we have a drop attached to a wall.

After chapter 2 we turn our attention to the problem of slow flow around rigid particles in a viscous fluid, which has been the target application for most of the work in this thesis. This kind of flow can be found in e.g. particle suspensions and porous media. The physics of the problem can be described by Stokes equations, which are a simplification of Navier-Stokes equations. This allows the problem to be formulated as a boundary integral equation, which we do in chapter 3. In chapter 4 we show how the solution of the integral equation can be accelerated through the method of Ewald summation, when solving for large, periodic particle systems. In chapter 5 we continue discussing Ewald summation, giving an overview of the available methods for deriving decompositions, and showing how these methods are related to each other. Finally, in chapter 6 we turn to the concept of quadrature, which is fundamental to boundary integral methods. We discuss an efficient method

for estimating quadrature errors, and introduce the method which we have used to deal with the special integrals that appear in the context of boundary integrals.

Chapter 2

Multiphase flow, surfactants and wetting

Multiphase flow refers to flow situations including two (or more) fluids, which are separated by an interface. Examples of such interfaces are the surfaces of ink drops in an inkjet printer and gas bubbles in boiling water, and the surfaces separating oil from water in an emulsion, such as milk or mayonnaise. We will here not make the distinction between *multiphase* (one fluid in different phases) and *multicomponent* (different fluids) flows, but rather just consider systems where the fluids involved are immiscible and there is no phase change taking place.

In microfluidic applications, and particularly in lab-on-a-chip devices, multiphase flows are commonplace. Drops are often used as atomic units of fluid for analysis or chemical reactions, and it is therefore important to understand and be able to control how drops form, coalesce, move and break up as they move through the device [92, 109]. However, surface tension and wall effects are dominant at the scales in question, due to the large surface-to-volume effects. This makes the fluids behave quite differently from what we are used to observing on the macroscale, which is why numerical simulations are an important tool for understanding and developing the flows in microfluidic devices.

In Paper I we present a method for two-phase flow with surfactants and contact line dynamics in two dimensions. Here we give an introduction to the concepts involved, as well as a brief overview of the available numerical methods.

2.1 Multiphase flow

Governing equations

For the setting of multiphase flow, we limit ourselves to two-dimensional flow, which is a valid simplification in many microfluidic applications. We consider the Navier-Stokes equations in non-dimensional form for the velocity and pressure fields $\mathbf{u}$ and

P,

$$\frac{\partial \mathbf{u}}{\partial t} + (\mathbf{u} \cdot \nabla)\mathbf{u} = -\nabla P + \frac{1}{\text{Re}}\nabla^2 \mathbf{u} + \frac{1}{\text{ReCa}}\mathbf{f},$$

$$\nabla \cdot \mathbf{u} = 0.$$

(2.1)

The Reynolds number $\text{Re} = \frac{\rho U L}{\mu}$ expresses the ratio of inertial to viscous forces for a liquid of density ρ and viscosity μ in a flow with characteristic length L and characteristic velocity U. The capillary number $\text{Ca} = \frac{\mu U}{\sigma}$ expresses the ratio of viscous to surface tension forces, where σ is the surface tension (or surface energy). The body forces of the system, represented by $\mathbf{f}$, are on the microscale completely dominated by the surface tension, so gravity can be neglected unless we are considering bubbles rising under buoyancy forces. The surface tension force can for a clean interface be expressed as [16],

$$\mathbf{f}(\mathbf{x}) = \begin{cases} \sigma \kappa \hat{\mathbf{n}}, & \mathbf{x} \in \Gamma, \\ 0, & \mathbf{x} \notin \Gamma, \end{cases}$$

(2.2)

where κ is the local curvature of the interface and $\hat{\mathbf{n}}$ is the normal vector. The interface Γ can in two dimensions naturally be viewed as a closed curve, which we parameterize in the arc length s. The time-dependence of the interface can then in Lagrangian form be expressed as an ODE,

$$\frac{\mathrm{d}\Gamma(s)}{\mathrm{d}t} = \mathbf{u}(\Gamma(s), t).$$

(2.3)

The velocity field $\mathbf{u}(\Gamma(s), t)$ is evaluated at the position of the interface and is governed by (2.1), which in turn is coupled to the interface through (2.2).

Numerical methods

The system which we describe in (2.1), (2.2) and (2.3) is seemingly simple, yet presents many computational difficulties. A large number of computational methods for multiphase flow have been developed since the beginning of the 1990's, all with the purpose of circumventing limitations of previous methods. There now exists a wide range of methods, all with different advantages. Which method is used in practice depends highly on the application at hand, and also on the availability of codes, since implementing a state-of-the-art method for multiphase flow is a demanding task. We here give a brief overview of some of the existing methods, and discuss the difference between explicit and implicit interface representations. For a more in-depth introduction to computational methods for multiphase flow, we refer to the review by Wörner [104].

Common to most multiphase methods for finite Reynolds number flows is that the flow field is computed on an Eulerian grid, either by solving the Navier-Stokes equations (2.1) or by using a lattice Boltzmann method [25], which solves a

mesoscale approximation of the Navier-Stokes equations. The task is then to solve the problem of tracking the interface Γ as it moves by (2.3), compute the surface tension force (2.2) on the interface and then evaluate the force on the grid. The essential difficulty in interface tracking is that the dimensionality of the interface is one less than the domain of the flow, meaning that the interface in practice never coincides with the Eulerian grid, if a fixed grid is used.

For zero Reynolds number flows, also known as Stokes flow or creeping flow, it is possible to use a boundary integral method instead of a grid-based method. This will be discussed further in chapter 3, though not in the setting of multiphase flow.

Explicit interface representation

In explicit interface tracking methods, the coordinates of the interface are explicitly tracked as the interface evolves. The most prominent of these methods is the front-tracking method [99, 101], where the interface is represented by a discrete set of marker points. These points need to be redistributed as the interface evolves, to maintain an accurate interpretation of the interface. This is relatively simple to implement in two dimensions, but more challenging in three dimensions, as the bookkeeping of the interface representation becomes more involved. The connection between the Lagrangian interface representation and the Eulerian grid is in the front-tracking method obtained by interpolation using regularized delta functions, which were introduced in the immersed boundary method by Peskin [73, 74, 65].

A way of using an explicit interface tracking without having to interpolate between the interface and grid is to use a moving mesh method [36, 69, 81, 80], where the flow equations are solved on an unstructured grid, which is adapted to follow the interface at every time step. This allows the interface to be explicitly tracked, but requires efficient algorithms for automatically refining and coarsening the grid, especially in the case of large interface deformations.

A feature which is common to all explicit interface tracking methods is that one must explicitly treat topological changes to the interface, such as breakup and coalescence of drops. This requires extra modeling and additional implementation difficulties, but also allows for an accurate treatment of such phenomena, given a valid model.

Implicit interface representation

In implicit interface tracking methods, the location of the interface is not explicitly advected from one time step to another. Instead, the interface position is in each time step recovered from a scalar quantity, which is advected on an Eulerian grid. Such methods include volume of fluid [87], level set [88], conservative level set [71], phase field [5] and lattice Boltzmann [4].

Topological changes are handled automatically in all implicit interface tracking methods, although this behavior is not always physically motivated. The case

of coalescence appears to be particularly troublesome, as the so-called numerical coalescence creates results that differ from experiments [104].

2.2   Surfactants

Surfactants, or surface active agents, are molecules which adhere to the interfaces in multiphase flows, where they lower the surface tension. They occur in many systems, either by design (e.g. detergents), naturally (e.g. pulmonary surfactant [105]) or as contaminants, and can drastically affect the dynamics of drops and bubbles when present [91, 95]. Surfactants are classified as either soluble or insoluble, depending on if they can be present as a concentration both in the bulk fluid and on the interface, or just as a concentration on the interface. Insoluble surfactants can be modeled as a scalar concentration ρ, which is present on the interface Γ and governed by an advection-diffusion equation on the interface [90],

$$\frac{\mathrm{D}\rho}{\mathrm{D}t} + \rho(\nabla_s \cdot \mathbf{u}) = \frac{1}{\mathrm{Pe}_\Gamma}\nabla_s^2\rho, \quad \mathbf{x} \in \Gamma, \tag{2.4}$$

where ∇_s is the surface gradient operator, which in two dimensions can be expressed as $\nabla_s = \hat{\boldsymbol{\tau}}\frac{\mathrm{d}}{\mathrm{d}s}$, and Pe_Γ is the Peclet number, governing surfactant diffusion on the interface. Soluble surfactants are also governed by an additional advection-diffusion equation in the domain, together with source terms linking the bulk concentration to the interface concentration [15].

The presence of a surfactant concentration $\rho(s)$ on the interface creates local variations in the surface tension σ. This can be modeled through the Langmuir equation of state [72], here stated in non-dimensional form,

$$\sigma(s) = 1 + \mathrm{E}\ln(1 - \rho(s)),$$

where E is the dimensionless elasticity number, expressing to what extent surfactants modify the surface tension. This local variation in surface tension has a secondary effect; it generates a tangential force at the interface, proportional to the surfactant gradient on the surface. This force is known as the Marangoni stress, and it is central to many of the phenomena which are associated with surfactants. The full surface force at the interface is then

$$\mathbf{f} = \sigma\kappa\hat{\mathbf{n}} + \frac{\mathrm{E}}{1 - \rho}\frac{\mathrm{d}\rho}{\mathrm{d}s}\hat{\boldsymbol{\tau}}, \quad \mathbf{x} \in \Gamma.$$

Simulating flows with surfactants involves representing the concentration ρ and solving (2.4) on the interface Γ, which is more natural in an explicit interface representation. There are however numerical methods for multiphase flows with surfactants using both explicit and implicit interface representations, and there has been much development in this area in recent years [2, 53, 61, 67, 96, 106].

2.3 Wetting

When the interface between two fluids comes into contact with a solid surface, there is a contact line (or point, in 2D), along which the three components meet. A simple example of a contact line is the intersection between glass, water and air that encircles a drop lying on a glass plate. The angle θ between the fluid-fluid interface and the solid is called the contact angle (see Figure 2.1). When the system is at rest, the surface energies $\sigma_1, \sigma_2, \sigma$ at the fluid-fluid and solid-fluid interfaces will be in horizontal equilibrium, which is formulated by Young's equation [28] for the static contact angle θ_s,

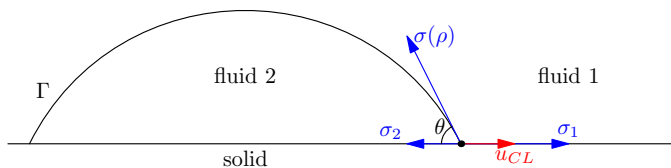$$\sigma_1 - \sigma_2 - \sigma \cos \theta_s = 0.$$

Figure 2.1: Drop wetting a solid surface, forming a contact angle θ between the surface and interface.

The case of dynamic wetting, when the contact line is moving on the solid with a velocity u_{CL}, is very common in many practical applications. However, it is also much more complicated than the static case. The Navier-Stokes equations with the standard no-slip boundary condition result in an infinite shear stress at the contact line, so additional modeling is required (see reviews by Blake [13] and Bonn et al. [14]). This makes numerical simulation of moving contact lines difficult, since one has to choose some kind of (more or less physical) model for the movement of the contact line. Nevertheless, simulations of wetting flows have been performed with good results, see for example Muradoglu & Tasoglu [66], Zahedi et al. [108] and Carlson et al. [24].

2.4 Simulating wetting flows with surfactants

In Paper I, we present a method for simulating two-phase flow with moving contact lines and insoluble surfactants in two dimensions. The method is based on an explicit interface tracking method developed by Khatri & Tornberg [53] and Lindbo & Tornberg [58, Paper V], where the interface is divided into segments, which are each represented by a function in a local coordinate frame (see Figure 2.2). This representation is natural for solving the surfactant PDE (2.4) on the interface, and also for representing open interfaces. To drive the motion of the contact line, we

apply a boundary condition derived by Ren & E [83], relating the contact line velocity u_{CL} to the contact angle θ. Figure 2.3 shows an example of the results.
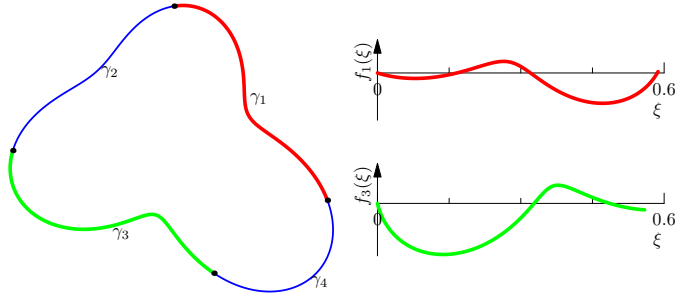
Figure 2.2: Interface (left), which is divided into segments. The segments are then represented in a local coordinate frame (right).
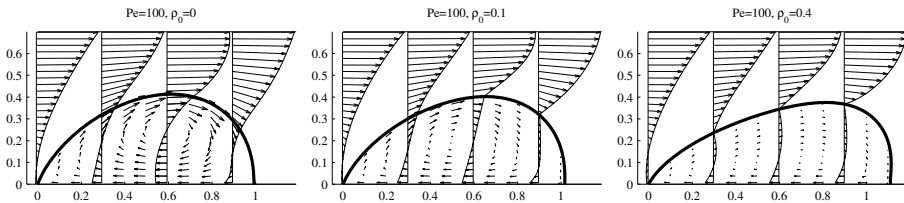
Figure 2.3: Drop on a solid surface in shear flow. To the left is a clean drop, with a velocity profile that is smooth across the interface. To the right is a drop with surfactants. The shear flow creates a surfactant gradient on the interface, resulting in Marangoni forces that cause a kink in the velocity profile across the interface.

Chapter 3

Stokes flow and periodic suspensions

In most microfluidic applications, effects due to fluid viscosity dominate over effects due to fluid intertia, as was mentioned in chapter 1. This is measured by the Reynolds number, $\text{Re} = \frac{\rho U L}{\mu}$, which describes the ratio of inertial to viscous forces for a liquid of density ρ and viscosity μ in a flow with characteristic length L and velocity U. For self-propelling microorganisms, such as swimming bacteria, the Reynolds number is on the order of 10^{-4} or 10^{-5} [78]. In such cases, when $\text{Re} \ll 1$, it is valid to linearize the Navier-Stokes equations (2.1) by assuming that $\text{Re} = 0$. The nonlinear convective term of the equations then disappears, and one obtains the linearized Stokes equations[1],

$$
\begin{aligned}
-\nabla P + \mu \nabla^2 \mathbf{u} + \mathbf{f} &= 0, \\
\nabla \cdot \mathbf{u} &= 0,
\end{aligned}
\tag{3.1}
$$

where $\mathbf{u}$ is velocity, P pressure and $\mathbf{f}$ body force. The lack of time-dependence in (3.1) implies that the flow at any given time is completely determined by the boundary conditions. This can be viewed as the fluid having no "memory", which is a natural consequence of the assumption that it has no inertia.

A practical problem involving Stokes flow appears in the study of sedimentation, which is the process that occurs naturally when a suspension of microparticles is left to rest. Unless the particles are neutrally buoyant, gravity will cause them to sink (sediment) slowly. Stokes equations are valid for this problem due to the small size of the particles and the low velocities involved. The sedimentation takes place on the microscale, yet it affects the macroscopic properties of the suspension. Understanding the sedimentation behavior of particles — and how it depends on their shape and volume fraction — is of value for scientists and engineers working

---

[1]We refer to Pozrikidis [76] for a complete version of the brief introduction to Stokes flow given here.

with suspensions. It is also surprisingly difficult [42], and has been a field of active research for many years [27, 43].

When studying sedimentation, one is typically interested in how a suspension behaves in a container that is very large compared to the particle size, such that effects from the container walls are not seen. However, the hydrodynamic interactions between particles are in Stokes flow very long-range (decay as the inverse of the distance), so in simulations a very large domain is required if one wants to avoid boundary effects due to the domain being of finite size. The classic remedy for this is to use periodic boundary conditions, which means that one only considers particles in a box (also called the primary cell) of dimensions $L_1 \times L_2 \times L_3$, and then requires the flow and pressure gradient fields to be periodic with respect to that box,

$$\mathbf{u}(\mathbf{x}) = \mathbf{u}(\mathbf{x} + \boldsymbol{\tau}(\mathbf{p})),$$
$$\nabla P(\mathbf{x}) = \nabla P(\mathbf{x} + \boldsymbol{\tau}(\mathbf{p})),$$

where

$$\boldsymbol{\tau}(\mathbf{p}) = (p_1 L_1, p_2 L_2, p_3 L_3), \quad \mathbf{p} \in \mathbb{Z}^3.$$

Physically, this is equivalent to considering the flow around a particle lattice, whose structure is given by the positions of the particles in the primary cell.

3.1   Numerical methods

To study sedimentation using computer simulation, a numerical method is needed for computing Stokes flow around a set of rigid particles, using periodic boundary conditions. In particular, we are interested in computing the rigid body motion of the particles as they sediment. For spherical particles, this can be done efficiently using the method of Stokesian Dynamics by Brady & Bossis [17], which approximates the hydrodynamic many-body interactions using the known solutions for the interactions between two spheres. This has no straightforward extension to non-spherical particles, so then the Stokes equations have to be solved. The methods available for this can be divided into two main classes: volume methods and boundary integral methods.

Volume methods

In a volume method, the entire domain is discretized using a (structured or unstructured) grid, and then an approximate solution to the Stokes equations (3.1) is computed on that grid. A large number of methods are available for this, such as finite difference (FD) methods, finite element (FE) methods, spectral methods and lattice Boltzmann (LB) methods [103, 23, 25]. Using a grid with a characteristic

cell length h, these methods generate a system with $N = \mathcal{O}\left(h^{-3}\right)$ degrees of freedom. This system is typically sparse, and can be solved in $\mathcal{O}\left(N\right)$ time using e.g. a multigrid method [64].

The difficulty with using volume methods for the current problem is that a no-slip boundary condition must be enforced on the surface of the particles, which are moving through the domain. This is closely related to the difficulties encountered when using an explicit interface representation in a multiphase flow simulation, as was discussed in chapter 2, and the solution strategies are essentially the same. When using an FE method with an unstructured grid, one can track the particles using an arbitrary Lagrangian-Eulerian (ALE) formulation [93]. This allows the boundary conditions to be accurately represented, but requires a grid that follows the particles. Maintaining such a grid quickly becomes very complex as a large number of particles move through the domain, sometimes getting very close to each other. Alternatively, one can use a fixed, structured grid and somehow enforce the boundary conditions on that grid. Using an FD/FE method, this can be done using an immersed boundary method, where the volume grid and the particle grid interact through a regularized delta function [100, 21, 52, 37]. In an LB method, this can be done by locally using a suitable bounce-back scheme [49]. All of these methods have been successfully used for simulating particle sedimentation. However, they all share the limitation of being restricted to low order, which means that the number of degrees of freedom grows rapidly when the error tolerance is decreased.

Boundary integral methods

A benefit of working with the Stokes equations instead of the full Navier-Stokes equations is that they belong to the class of linear PDEs with constant coefficients. This implies that the flow in a domain can be represented using a surface integral over the boundaries, assuming the boundaries Lyapunov smooth. The problem of solving Stokes equations in the domain ($\mathbb{R}^3$) is then reduced to the problem of solving a boundary integral equation on the particle surfaces ($\mathbb{R}^2$). Discretizing the surfaces using a characteristic grid length h, the number of degrees of freedom N becomes $\mathcal{O}\left(h^{-2}\right)$. Since no volume grid is required, the issue of handling the particles' movement through the domain is greatly simplified; all that is needed is a Lagrangian tracking of the rigid body motion of the surface grids.

Several different methods exist for solving the integral equation resulting from the boundary integral representation. Using a collocation or Galerkin method, an approximate solution is found in the space spanned by a given set of basis functions. This approach is often used in boundary element methods, which are able to deal with complicated geometries by using a piecewise discretization of the boundary. Alternatively, one can use the Nyström method, where the integral equation is enforced at the quadrature nodes. This method is very straightforward to implement on smooth, parametric surfaces, such as the spheroids considered in this thesis. For a thorough discussion of these methods, we refer to Atkinson [6].

Regardless of which solution method is used, two important components are required if a boundary integral method is to be competitive with volume methods: fast evaluation and accurate quadrature.

A fast evaluation method is required because the linear system corresponding to the integral equation is dense. A direct solution of this system would then have an $\mathcal{O}\left(N^3\right)$ cost, which is prohibitively expensive. Fortunately, the system is suitable for iterative solution, and can with the right formulation and preconditioning be made to converge in a number of iterations that is independent of N. Still, at every iteration the cost of one left hand side evaluation (the matrix vector product, or *matvec*) is $\mathcal{O}\left(N^2\right)$ due to the dense matrix structure. To reduce the cost of one matvec, a fast method is required for evaluating it. Two classes of such methods are fast multipole methods [41] and fast Ewald methods (further discussed in chapter 4). They reduce the matvec cost to $\mathcal{O}\left(N\right)$ or $\mathcal{O}\left(N \log N\right)$, such that the total solution cost is $\mathcal{O}\left(h^{-2}\right)$ or $\mathcal{O}\left(h^{-2} \log h\right)$ when combined with an iterative method. This makes boundary integral methods competitive with volume methods, which have an $\mathcal{O}\left(h^{-3}\right)$ complexity. It is worth noting that this advantage over volume methods is in part due to the fact that we do not explicitly need the solution in the domain; for the sedimentation problem we only need the solution on the particle surfaces. However, once we have solved the boundary integral equation we can evaluate the solution anywhere in the domain. The cost for this is then at least $\mathcal{O}\left(N + N_e\right)$, where N_e is the number of evaluation points.

Accurate quadrature is required because the accuracy of a boundary integral method is dictated by the accuracy of the underlying quadrature rule. For smooth surfaces and integrands, formulating an exponentially convergent quadrature is straightforward, using e.g. the trapezoidal or Gauss-Legendre rules. In a boundary integral formulation, however, the integrands encountered are typically singular or nearly singular. This requires the use of specialized quadrature methods, which are central to the field of boundary integral methods. Such methods are further discussed in chapter 6 of this thesis. Once implemented, they allow the boundary integral equation to be solved to high accuracy using a limited number of degrees of freedom, due to the high order of accuracy of the quadrature methods.

In the remainder of this chapter we introduce a boundary integral formulation for Stokes flow, which forms the foundation for the fast and accurate boundary integral framework developed in this thesis.

3.2   Boundary integral formulation

We are concerned with external flow outside a body with surface Γ, located in the infinite domain D_e. Starting from the Lorentz reciprocal theorem, one can derive the boundary integral representation of the flow for $\mathbf{x} \in D_e$ [76, p. 27]. Given the

velocity $\mathbf{u}$ and force $\mathbf{f}$ on Γ, we can then write

$$
u_j(\mathbf{x}) = -\frac{1}{8\pi\mu} \int_\Gamma f_i(\mathbf{y}) G_{ij}(\mathbf{x}, \mathbf{y}) \mathrm{d}S(\mathbf{y})
$$
$$
-\frac{1}{8\pi} \int_\Gamma u_i(\mathbf{y}) T_{ijk}(\mathbf{x}, \mathbf{y}) \hat{n}_k(\mathbf{y}) \mathrm{d}S(\mathbf{y}), \tag{3.2}
$$

under the assumption that $|\mathbf{u}| = \mathcal{O}(|\mathbf{x}|^{-1})$ and $p = \mathcal{O}(|\mathbf{x}|^{-2})$ as $|\mathbf{x}| \to \infty$. The unit vector $\hat{\mathbf{n}}$ is the outward pointing normal. The kernels T and G are the stresslet and stokeslet fundamental singularities,

$$
T_{ijk}(\mathbf{x}, \mathbf{y}) = -6\frac{r_i r_j r_k}{r^5}, \tag{3.3}
$$

$$
G_{ij}(\mathbf{x}, \mathbf{y}) = \frac{\delta_{ij}}{r} + \frac{r_i r_j}{r^3}, \tag{3.4}
$$

where $\mathbf{r} = \mathbf{x} - \mathbf{y}$ and $r = |\mathbf{r}|$. The two integrals in the boundary integral representation (3.2) are called the single and double layer potentials, and both can be used independently to represent Stokes flow. This is commonly referred to as generalized boundary integral representations [76].

Keeping only the single layer potential and letting $\mathbf{x} \to \Gamma$, by enforcing a Dirichlet boundary condition on $\mathbf{u}$ we obtain a weakly singular Fredholm equation of the first kind for an unknown single layer density $\mathbf{f}$,

$$
-\frac{1}{8\pi\mu} \int_\Gamma f_i(\mathbf{y}) G_{ij}(\mathbf{x}, \mathbf{y}) \mathrm{d}S(\mathbf{y}) = \mathbf{u}(\mathbf{x}), \quad \mathbf{x} \in \Gamma. \tag{3.5}
$$

The single layer formulation (3.5) is ill-conditioned, in the sense that the condition number is unbounded [39]. However, it is still usable for simulations, see [48, 44].

Keeping instead the double layer potential, we get the double layer representation for the velocity at a point in the domain, such that for a double layer density $\mathbf{q}$ on Γ,

$$
u_j(\mathbf{x}) = \int_\Gamma q_i(\mathbf{y}) T_{ijk}(\mathbf{x}, \mathbf{y}) \hat{n}_k(\mathbf{y}) \mathrm{d}S(\mathbf{y}). \tag{3.6}
$$

The actual values of $\mathbf{q}$ depend on how we define the double layer representation, so we are free to scale it with a constant, as we have done here for convenience. Taking the limit $\mathbf{x} \to \Gamma$, the double layer potential contains a jump,

$$
\lim_{\epsilon \to 0} u_j(\mathbf{x} \pm \epsilon \hat{\mathbf{n}}) = \mp 4\pi \mathbf{q}(\mathbf{x}) + \int_\Gamma q_i(\mathbf{y}) T_{ijk}(\mathbf{x}, \mathbf{y}) \hat{n}_k(\mathbf{y}) \mathrm{d}S(\mathbf{y}). \tag{3.7}
$$

Enforcing a no-slip boundary condition on the surface, we get a Dirichlet boundary condition for $\mathbf{u}$ (which is homogeneous if the surface is stationary). Letting $\mathbf{x} \to \Gamma$ from the exterior, we then get a weakly singular Fredholm equation of the second kind for an unknown density $\mathbf{q}$,

$$
u_j(\mathbf{x}) = -4\pi \mathbf{q}(\mathbf{x}) + \int_\Gamma q_i(\mathbf{y}) T_{ijk}(\mathbf{x}, \mathbf{y}) \hat{n}_k(\mathbf{y}) \mathrm{d}S(\mathbf{y}), \quad \mathbf{x} \in \Gamma. \tag{3.8}
$$

Once we have solved (3.8) for $\mathbf{q}$, we can evaluate the solution anywhere in the domain using (3.6).

The singularity in the right hand side of (3.8) can be treated by the method of singularity subtraction. One then applies the identity

$$\int_\Gamma T_{jlm}(\mathbf{x},\mathbf{y})\hat{n}_m(\mathbf{y})\mathrm{d}S(\mathbf{y}) = \delta_{jl} \begin{cases} 0, & \mathbf{x} \text{ outside } \Gamma, \\ 4\pi, & \mathbf{x} \in \Gamma, \\ 8\pi, & \mathbf{x} \text{ inside } \Gamma, \end{cases}$$

allowing us to restate (3.8) as

$$u_j(\mathbf{x}) = \int_\Gamma \left(q_i(\mathbf{y}) - q_i(\mathbf{x}) \right) T_{ijk}(\mathbf{x},\mathbf{y})\hat{n}_k(\mathbf{y})\mathrm{d}S(\mathbf{y}), \quad \mathbf{x} \in \Gamma. \tag{3.9}$$

Working with (3.9), we can simply skip the term $\mathbf{y} = \mathbf{x}$ in numerical quadrature, since the integrand goes to zero as $\mathbf{y} \to \mathbf{x}$ (assuming $\mathbf{q}$ smooth). This reduces the order of the singularity in a way that gives third order convergence [Paper II]. More elaborate ways of dealing with the singularity will be discussed in chapter 6.

The advantage of the double layer formulation — compared to the single layer formulation — is that it is well-conditioned, in the sense that its condition number is bounded. The drawback is however that the double layer potential alone is incomplete, since it can only represent external flows which have zero net force and torque on the surface Γ. There are various remedies for this, as discussed by Gonzalez [39]. We have used the completed double layer formulation of Power & Miranda [75], where two singular flow solutions (a stokeslet $\mathbf{f}$ and a rotlet $\mathbf{t}$) located at an arbitrary point $\mathbf{x}_c$ inside Γ are added to the double layer representation (3.6), to generate a completion flow that is able to represent net force and torque. The velocity representation then becomes,

$$u_j(\mathbf{x}) = \int_\Gamma q_i(\mathbf{y})T_{ijk}(\mathbf{x},\mathbf{y})\hat{n}_k(\mathbf{y})\mathrm{d}S(\mathbf{y})$$
$$+ \underbrace{\frac{1}{8\pi\mu} \left(G_{ij}(\mathbf{x},\mathbf{x}_c)f_j + R_{ij}(\mathbf{x},\mathbf{x}_c)t_j \right)}_{\text{completion flow}}, \tag{3.10}$$

where R is the rotlet fundamental singularity,

$$R_{ij}(\mathbf{x},\mathbf{y}) = \epsilon_{ijk}\frac{r_k}{r^3}. \tag{3.11}$$

A common choice for the source point $\mathbf{x}_c$ is to use the center of the volume enclosed by Γ.

3.3 Mobility and resistance problems

When considering the problem of a rigid body in Stokes flow, the fundamental quantities of interest are its external forcing $(\mathbf{f}, \mathbf{t})$ and its rigid body motion $(\mathbf{V}, \mathbf{\Omega})$.

Depending on which quantities are given, the problem is classified as being either a *resistance problem* or a *mobility problem*. In a resistance problem, the rigid body motion is known and the external forcing is sought. The completion flow is then formed by expressing **f** and **t** as functionals of the double layer density **q** [75]. In a mobility problem, the situation is the inverse. The external forcing on the body is then known, and one seeks to compute its rigid body motion. The completion flow is then known, and one instead has to express **V** and **Ω** as functionals of **q** [76, p. 138].

3.4 Periodic boundary conditions

As mentioned in the beginning of the chapter, periodic boundary conditions are useful when one wants to simulate very large particle systems. When using a boundary integral method, this however means that the velocity at a point is determined by the integral over all periodic images of all particle surfaces, all the way up to infinity. The sum over all periodic images does not converge unless treated correctly, and then it converges very slowly. To make the evaluation of this integral computationally attainable, a fast method is therefore required. In molecular dynamics, the similar problem of computing a lattice sum of electrostatic potentials is solved by using fast Ewald summation methods, which are also applicable to the problem of periodic Stokes flow. We will in the following section outline how to formulate the completed double layer representation (3.10) for periodic boundary conditions, while Ewald summation will be further discussed in chapter 4

Let us now consider a primary cell with N_p rigid particles, having surfaces Γ_α and centers of mass $\mathbf{x}_c^{(\alpha)}$, $\alpha = 1, ..., N_p$. Each particle is subject to a net force $\mathbf{f}^{(\alpha)}$ and a net torque $\mathbf{t}^{(\alpha)}$ (through either a mobility or resistance formulation). Introducing the periodic double layer potential from a surface Γ,

$$\mathcal{W}_j[\Gamma, \mathbf{q}](\mathbf{x}) = \sum_{\mathbf{p}\in\mathbb{Z}^3} \int_\Gamma q_l(\mathbf{y}) T_{jlm}(\mathbf{x}, \mathbf{y} + \boldsymbol{\tau}(\mathbf{p})) \hat{n}_m(\mathbf{y}) \mathrm{d}S(\mathbf{y}), \qquad (3.12)$$

and the periodic completion potential from point sources **f** and **t** located at $\mathbf{x}_c$,

$$\mathcal{V}_j[\mathbf{x}_c, \mathbf{f}, \mathbf{t}](\mathbf{x}) = \sum_{\mathbf{p}\in\mathbb{Z}^3} \frac{1}{8\pi\mu} \Big(G_{jm}(\mathbf{x}, \mathbf{x}_c + \boldsymbol{\tau}(\mathbf{p})) f_m + $$
$$R_{jm}(\mathbf{x}, \mathbf{x}_c + \boldsymbol{\tau}(\mathbf{p})) t_m \Big), \qquad (3.13)$$

the periodic form of the completed double layer representation can be written

$$u_j(\mathbf{x}) = \sum_{\alpha=1}^{N_p} \Big(\mathcal{W}_j[\Gamma_\alpha, \mathbf{q}](\mathbf{x}) + \mathcal{V}_j[\mathbf{x}_c^{(\alpha)}, \mathbf{f}^{(\alpha)}, \mathbf{t}^{(\alpha)}](\mathbf{x}) \Big). \qquad (3.14)$$

The interpretation of this is that the flow at a point **x** is influenced by all periodic images of all particles in the primary cell, and that the influence is long-range,

since it decays as $1/r$. On the surface Γ_α of each particle we set a no-slip boundary condition. For a rigid body with center of mass $\mathbf{x}_c^{(\alpha)}$ and translational and rotational velocities $\mathbf{V}^{(\alpha)}$ and $\mathbf{\Omega}^{(\alpha)}$, this implies that

$$\mathbf{u}(\mathbf{x}) = \mathbf{U}^{(\alpha)}(\mathbf{x}) := \mathbf{V}^{(\alpha)} + \mathbf{\Omega}^{(\alpha)} \times (\mathbf{x} - \mathbf{x}_c^{(\alpha)}), \quad \mathbf{x} \in \Gamma_\alpha.$$

Now we let $\mathbf{x}$ in (3.14) go to the surface Γ_β of one body, and apply the double layer jump (3.7). We then obtain the boundary integral formulation for the unknown density $\mathbf{q}$ for our periodic system of particles,

$$-4\pi\mathbf{q}(\mathbf{x}) + \sum_{\alpha=1}^{N_p} \left(\mathcal{W}_j[\Gamma_\alpha, \mathbf{q}](\mathbf{x}) + \mathcal{V}_j[\mathbf{x}_c^{(\alpha)}, \mathbf{f}^{(\alpha)}, \mathbf{t}^{(\alpha)}](\mathbf{x}) \right) = U_j^{(\beta)}(\mathbf{x}), \quad (3.15)$$

$$\mathbf{x} \in \Gamma_\beta, \quad \beta = 1, ..., N_p.$$

The system is closed by adding constitutive equations relating $\mathbf{q}$ to either $\mathbf{V}^{(\alpha)}$ and $\mathbf{\Omega}^{(\alpha)}$ (mobility problem) or $\mathbf{f}^{(\alpha)}$ and $\mathbf{t}^{(\alpha)}$ (resistance problem).

To solve the system (3.15) numerically, we discretize the surface integrals using a quadrature rule with weights w_j, such that for a function $g(\mathbf{x})$

$$\sum_{\alpha=1}^{N_p} \int_{\Gamma_\alpha} g(\mathbf{x})\mathrm{d}S(\mathbf{x}) \approx \sum_{\alpha,j} w_j^{(\alpha)} g(\mathbf{x}_j^{(\alpha)}) = \sum_{s=1}^{N} w_s g(\mathbf{x}_s), \quad (3.16)$$

where the sum $s = 1, ..., N$ goes over all discretization points on all bodies in the primary cell. In chapter 6 we discuss how to formulate this quadrature rule. Applying the Nyström method, we require the discrete version of (3.15) to be satisfied at the discrete points,

$$-4\pi\mathbf{q}(\mathbf{x}_t) + \sum_{\alpha=1}^{N_p} \mathcal{W}_j^h[\Gamma_\alpha, \mathbf{q}](\mathbf{x}_t) + \sum_{\alpha=1}^{N_p} \mathcal{V}_j[[\mathbf{x}_c^{(\alpha)}, \mathbf{f}^{(\alpha)}, \mathbf{t}^{(\alpha)}](\mathbf{x}_t) = U_j(\mathbf{x}_t),$$

$$t = 1, ..., N,$$

where $\mathcal{W}^h$ is the double layer potential evaluated using the quadrature rule (3.16). This is a dense $3N \times 3N$ system which is non symmetric and well-conditioned, and therefore suitable for iterative solution using the GMRES algorithm [84]. Before that can be done however, a fast method for evaluating the periodic sums in (3.12) and (3.13) must be applied. This is where the subject of Ewald summation enters the picture, as we will see in the next chapter.

Chapter 4

Ewald summation

As we saw in the previous chapter, formulating a boundary integral equation for a periodic suspension of sedimenting particles in Stokes flow results in a system where each particle is influenced by all other particles, all the way up to infinity. From the discretization of the periodic double layer potential (3.12) we get an infinite sum of stresslet potentials

$$
\begin{aligned}
u_j^{(T)}(\mathbf{x}) &:= \sum_{\alpha=1}^{N_p} \mathcal{W}_j^h[\Gamma_\alpha, \mathbf{q}](\mathbf{x}) \\
&= \sum_{s=1}^{N} \sum_{\mathbf{p} \in \mathbb{Z}^3} T_{jlm}\left(\mathbf{x} - \mathbf{x}_s + \tau(\mathbf{p})\right) q_l(\mathbf{x}_s) n_m(\mathbf{x}_s),
\end{aligned} \tag{4.1}
$$

where $\mathbf{n}(\mathbf{x}_s) = w_s \hat{\mathbf{n}}(\mathbf{x}_s)$ is the discrete form of the vector surface element $d\mathbf{S}$, and the stresslet T is defined in (3.3). The sum over all periodic images $\mathbf{p}$ has very slow decay, and furthermore it is only conditionally convergent, so direct evaluation of the sum is impractical. The standard remedy for this is to use Ewald summation, invented by P.P. Ewald [34] in 1921 for the computation of the electrostatic potential in periodic crystal lattices. The main idea behind the method is to decompose the periodic sum into two sums. One sum is designed to contain the singularity and converge rapidly, while the other is designed to be smooth, such that it converges rapidly in $\mathbf{k}$-space (Fourier space). In electrostatics, the potential $1/r$ is decomposed as

$$
\frac{1}{r} = \frac{1}{r} - \frac{\mathrm{erfc}(\xi r)}{r} + \frac{\mathrm{erfc}(\xi r)}{r} = \frac{\mathrm{erf}(\xi r)}{r} + \frac{\mathrm{erfc}(\xi r)}{r}.
$$

Figure 4.1 gives an illustration of how this works. The parameter ξ determines how fast the respective sums converge, and is used to balance the workload between them.
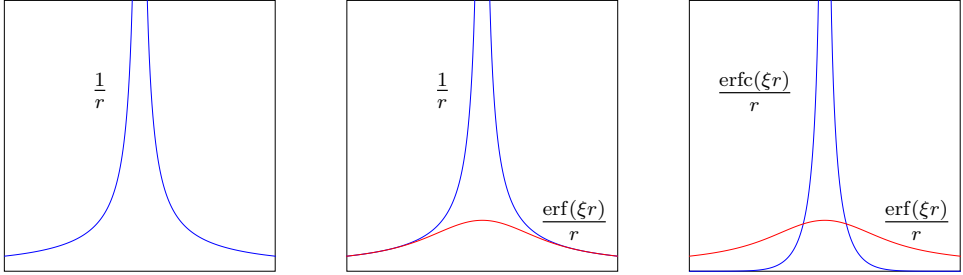
Figure 4.1: Illustration of how Ewald decomposition works. The original $1/r$ potential (left) is both long-range and singular. The long-range behavior is captured by the $\mathrm{erf}(\xi r)/r$ component (middle), such that the final decomposition (right) separates it from the singular part.

4.1   Stresslet decomposition

Ewald summation for the stresslet potential (4.1) builds on the same ideas as for the electrostatic potential, though the calculations are lengthier. An Ewald decomposition for the stresslet was first derived by Fan et al. [35], using the splitting method by Beenakker described in chapter 5. A second decomposition for stresslet, which has not to date been used in a practical application, was suggested by Marin [63, Paper IV]. We here introduce the decomposition by Fan et al., where the periodic sum (4.1) is decomposed as

$$
\begin{aligned}
u_j^{(T)}(\mathbf{x}) = {} & \sum_{s=1}^{N} \sum_{\mathbf{p}\in\mathbb{Z}^3} A_{jlm}(\xi, \mathbf{x} - \mathbf{x}_s + \tau(\mathbf{p})) S_{lm}(\mathbf{x}_s) \\
& + \frac{1}{V} \sum_{\mathbf{k}\neq 0} B_{jlm}(\xi, \mathbf{k}) e^{-k^2/4\xi^2} \sum_{s=1}^{N} S_{lm}(\mathbf{x}_s) e^{-i\mathbf{k}\cdot(\mathbf{x}-\mathbf{x}_s)} \\
& + \frac{1}{V} \sum_{s=1}^{N} T_{jlm}^{(0)}(\mathbf{x}_s) S_{lm}(\mathbf{x}_s),
\end{aligned} \tag{4.2}
$$

where $S_{lm} := q_l n_m$ and $V = L_1 L_2 L_3$. The first sum in (4.2) converges rapidly in real space, with A defined as

$$
\begin{aligned}
A_{jlm}(\xi, \mathbf{r}) :={} & C(\xi, \mathbf{r}) \hat{r}_j \hat{r}_l \hat{r}_m + D(\xi, \mathbf{r})(\delta_{jl}\hat{r}_m + \delta_{lm}\hat{r}_j + \delta_{mj}\hat{r}_l), \\
C(\xi, \mathbf{r}) ={} & -\frac{2}{r}\left(\frac{3}{r}\mathrm{erfc}(\xi r) + \frac{2\xi}{\sqrt{\pi}}(3 + 2\xi^2 r^2 - 4\xi^4 r^4)e^{-\xi^2 r^2}\right), \\
D(\xi, \mathbf{r}) ={} & \frac{8\xi^3 r}{\sqrt{\pi}}(2 - \xi^2 r^2)e^{-\xi^2 r^2}.
\end{aligned}
$$

The second sum in (4.2) converges rapidly in **k**-space, with B defined as

$$B_{jlm}(\xi, \mathbf{k}) := -i\frac{\pi}{k}\left[(\delta_{jl}\hat{k}_m + \delta_{lm}\hat{k}_j + \delta_{mj}\hat{k}_l) - 2\hat{k}_j\hat{k}_l\hat{k}_m\right]\left(8 + 2\frac{k^2}{\xi^2} + \frac{k^4}{\xi^4}\right).$$

The third sum in (4.2) is related to the $\mathbf{k} = 0$ term omitted from the **k**-space sum, and is derived in Paper II for periodic sedimentation of rigid bodies. It turns out that the choice,

$$T^{(0)}_{jlm}(\mathbf{y}) = 8\pi\delta_{lm}y_j,$$

results in a zero mean flow through the primary cell, which is what we want if we are to observe particles sedimenting through a quiescent fluid.

4.2 Truncation error estimates for the stresslet

While the real- and **k**-space sums in (4.2) are rapidly converging, they still have an infinite number of terms. We therefore need to truncate them at some point, and the question is where. Ideally, we would like to keep only the terms required to compute $\mathbf{u}^{(T)}$ to a certain tolerance ϵ, and discard the rest. This is a question of delicate balancing; compute too few terms and we lose precision, compute too many and we do unnecessary work.

For the Ewald sum of the electrostatic potential, Kolafa & Perram [55] developed an RMS (root mean squares) error estimate for the case of charges randomly distributed in the primary cell. Their derivation builds on making a statistical estimate of the error, but is nevertheless highly predictive and widely used. In Paper II, we use the reasoning of Kolafa & Perram to develop truncation error estimates for the stresslet, when decomposed using the Ewald decomposition by Fan et al. The estimates are for the error in RMS, defined as

$$e_{rms,j} := \sqrt{\frac{1}{N}\sum_{s=1}^{N}(u_j(\mathbf{x}_s) - \tilde{u}_j(\mathbf{x}_s))^2},$$

where $\mathbf{u}$ and $\tilde{\mathbf{u}}$ are the truncated and exact solutions, respectively. Both the real space and **k**-space estimates contain a factor $\sqrt{Q}$, which depends on the system involved. We find that for randomly distributed point stresslets, we get very accurate error estimates using the definition

$$Q := \sum_{s=1}^{N}\sum_{l=1}^{3}\sum_{m=1}^{3}q_l^2(\mathbf{x}_s)n_m^2(\mathbf{x}_s),$$

which sums the squared contributions from all the points. However, for the case of point sources related to quadrature of the double layer potential, using the above definition gives $Q \sim 1/N$ for a given geometry, with the number of discretization

points increasing with N. In practice we find that Q is constant as the number of quadrature points is increased, so we redefine it as

$$Q := \left(\sum_{\alpha=1}^{N_p} S_{\Gamma_\alpha} \right) \left(\sum_{l=1}^{3} \sum_{s=1}^{N} w_s q_l^2(\mathbf{x}_s) \right) \approx \sum_{\alpha=1}^{N_p} S_{\Gamma_\alpha} \sum_{l=1}^{3} \|q_l\|_2^2,$$

where $\| \cdot \|_2$ is the 2-norm, defined as

$$\|f\|_2^2 = \sum_{\alpha=1}^{N_p} \int_{\Gamma_\alpha} f^2(\mathbf{y}) \mathrm{d}S(\mathbf{y}).$$

Real space sum

In the real space sum the truncation is spatial, such that only points within a truncation radius r_c from the target point $\mathbf{x}$ are included in the sum. For a given radius r_c and Ewald parameter ξ, the RMS error is estimated as

$$e_{rms}^{(R)} \approx e^{-\xi^2 r_c^2} \sqrt{\frac{1}{27} \frac{Q}{V} \xi^2 r_c \left(327 + 1588\xi^2 r_c^2 - 1392\xi^4 r_c^4 + 448\xi^6 r_c^6 \right)},$$

by following the steps of Kolafa & Perram.

k-space sum

In the **k**-space sum, the truncation is on the reciprocal lattice, so we only compute the contribution from **k**-vectors within a box K, such that $|k_i| \leq K$. Deriving an estimate for the **k**-space truncation error turns out to be hard, but we heuristically find an error estimate that gives satisfactory results,

$$e_{rms}^{(F)} \approx e^{-K^2/4\xi^2 + 0.43K/\xi} \sqrt{\xi^2 L \frac{Q}{V}},$$

where $L = \min_i L_i$.

4.3   Other kernels

We have now seen how an Ewald summation can be formulated for the stresslet. To get a periodic double layer formulation, we also need the Ewald sums and corresponding error estimates for the stokeslet (3.4) and rotlet (3.11) potentials. The process of deriving these is completely analogous. For the stokeslet this can be found in Lindbo & Tornberg [59], while a derivation for the rotlet is included in Paper V.

4.4 Fast Ewald summation

We have so far discussed how the slowly converging sum over periodic images (4.1) can be cast into an Ewald sum (4.2), which converges very fast. However, even though it is rapidly converging, the Ewald sum is very expensive to compute in practice, since it has $\mathcal{O}\left(N^2\right)$ complexity with a constant that grows rapidly with increasing r_c and K. This complexity can be reduced to $\mathcal{O}\left(N \log N\right)$ by applying a mesh-based method, which allows the **k**-space sum to be computed using a fast Fourier transform (FFT). Such methods include the particle–particle–particle–mesh (P^3M), particle mesh Ewald (PME) and smooth particle mesh Ewald (SPME), all of which are introduced in a unified way by Deserno & Holm [29]. A quite recent contribution to this class of methods is the spectral Ewald (SE) method by Lindbo & Tornberg [59, 60], which uses scaled Gaussians instead of interpolation polynomials to create a grid representation of the pointwise charge density. This decouples the approximation error of the summation method from the truncation error of the Ewald sum, thus reducing the memory requirements of the method by allowing a minimal FFT grid to be used.

These mesh based fast Ewald methods are widely used for computing the long-range interactions in molecular simulations, but they have also been applied to hydrodynamic problems with Stokes flow. The PME method was used by Sierou & Brady [89] for their accelerated Stokesian dynamics (ASD), simulating suspensions containing up to 1000 spheres. Saintillan et al. [85] used SPME for sedimenting fiber suspensions, simulating systems of up to 512 fibers. Marin et al. [63, Paper III] used SE for the same problem, simulating up to 3800 fibers while using a more accurate fiber discretization. Recently, Wang & Brady [102] implemented the ASD method using SE instead of PME, resulting in the SEASD method.

In Paper II of this thesis we extend the spectral Ewald to work with the stresslet potential, and apply it for a suspension of sedimenting spheroid particles.

Chapter 5

Ewald decompositions

As we have seen in the previous chapter, Ewald summation is a very useful technique for summing periodic potentials which converge slowly, if at all, when summed directly. To apply the technique to a given potential, one first requires what is called an Ewald decomposition. The decomposition splits the potential into two parts, one which is short-ranged and converges rapidly in real space, and one which is smooth and converges rapidly in $\mathbf{k}$-space. As we shall see, decompositions are not unique, and there are several ways of constructing a decomposition of a given potential.

We will here describe two general approaches for creating decompositions, and show how they can be related to each other. We will then show how this relation can be used to create new decompositions with relatively little effort.

5.1 Splitting and screening

Given a PDE in free space (with the Laplace equation as an example in parentheses),

$$Lu = 4\pi q\delta, \quad (L = -\Delta),$$

we have a Green's function s.t.

$$u = qG, \quad (G = \frac{1}{r}).$$

In many cases, the Green's function can also be expressed as an operation K on r,

$$G = \mathrm{K}\, r, \quad (\mathrm{K} = \frac{1}{2}\Delta). \tag{5.1}$$

In a periodic setting, u will be computed by summing all periodic images of G. If G decays slowly $(1/r)$ an Ewald decomposition is required to compute the sum in a fast way. Such a decomposition can be obtained by splitting the operator K or by screening the Green's function G.

Splitting

The splitting method was invented by Beenakker [12] for the Rotne-Prager tensor, and later applied on the stokeslet by Pozrikidis [77], and on the stresslet by Fan & Phan-Thien [35]. The decomposition is obtained by introducing Φ and Θ, such that

$$\Phi + \Theta = r,$$

and writing

$$G^F + G^R = \mathrm{K}(\Phi + \Theta).$$

The real space part is obtained by applying K to Θ, which in general is a matter of differentiation,

$$G^R = \mathrm{K}\,\Theta,$$

while G^F is transformed to Fourier space,

$$\widehat{G}^F = \widehat{\mathrm{K}}\widehat{\Phi},$$

where $\widehat{\mathrm{K}}$ is the transformed operator (Laplace: $\widehat{\mathrm{K}} = -\frac{1}{2}k^2$). The Beenakker decomposition is obtained by setting

$$\Theta = r\,\mathrm{erfc}(\xi r),$$
$$\Phi = r\,\mathrm{erf}(\xi r),$$

having (see [77])

$$\widehat{\Phi} = \mathcal{F}[r\,\mathrm{erf}(\xi r)] = -\frac{8\pi}{k^4}\left(1 + \frac{1}{4}\frac{k^2}{\xi^2} + \frac{1}{8}\frac{k^4}{\xi^4}\right)e^{-k^2/4\xi^2}.$$

For the Laplace example, this yields

$$G^R = \frac{1}{2}\Delta\left(r\,\mathrm{erfc}(\xi r)\right) = \frac{\mathrm{erfc}(\xi r)}{r} + \frac{2\xi e^{-\xi^2 r^2}\left(\xi^2 r^2 - 2\right)}{\sqrt{\pi}},$$
$$\widehat{G}^F = -k^2\mathcal{F}[r\,\mathrm{erf}(\xi r)] = \frac{4\pi}{k^2}\left(1 + \frac{1}{4}\frac{k^2}{\xi^2} + \frac{1}{8}\frac{k^4}{\xi^4}\right)e^{-k^2/4\xi^2}.$$

This particular decomposition is however of limited interest, since it is more complicated than the classical Ewald decomposition for the Laplacian, and is likely to have slower convergence. The point here is that it is very simple to apply the Beenakker method, given K in (5.1).

Screening

Screening is done by introducing a screening function γ, $\|\gamma(\mathbf{x})\| = 1$, that decays smoothly away from zero. The decomposition of G is then obtained by adding and subtracting the convolution of G and γ,

$$G = G - (G * \gamma) + (G * \gamma),$$

such that

$$G^R = G - (G * \gamma),$$
$$\widehat{G}^F = \widehat{G}\widehat{\gamma}.$$

The classical Ewald decomposition for Laplace uses

$$\gamma_E(\mathbf{x}) = \xi^3 \pi^{-3/2} e^{-\xi^2 r^2} \quad \rightleftharpoons \quad \widehat{\gamma}_E(\mathbf{k}) = e^{-k^2/4\xi^2},$$

which leads to the decomposition

$$G^R = \frac{\operatorname{erfc}(\xi r)}{r}$$
$$\widehat{G}^F = \frac{4\pi}{k^2} e^{-k^2/4\xi^2}.$$

For the Stokeslet, the original derivation of the Ewald decomposition by Hasimoto [45] did not involve a screening function. However, it was later shown by Hernández-Ortiz et al. [48] that it is equivalent to applying the screening function

$$\gamma_H(\mathbf{x}) = \xi^3 \pi^{-3/2} e^{-\xi^2 r^2} \left(\frac{5}{2} - \xi^2 r^2 \right) \quad \rightleftharpoons \quad \widehat{\gamma}_H(\mathbf{k}) = e^{-k^2/4\xi^2} \left(1 + \frac{1}{4} \frac{k^2}{\xi^2} \right).$$

The screening method has one drawback, which is that evaluating the convolution $(G * \gamma)$ can be quite tedious. Reproducing the result by Hernández-Ortiz et al. requires a fair amount of calculations.

Relationship between methods

Screening and splitting can be viewed as two different ways of obtaining the same decomposition. There is then a relationship between (Φ, Θ) and γ, which can be explicitly expressed as

$$\mathrm{K}\,\Theta = G - (G * \gamma),$$
$$\widehat{\mathrm{K}}\widehat{\Phi} = \widehat{G}\widehat{\gamma}.$$

However, since $G = \mathrm{K}\, r$, we have the relationship

$$\widehat{G} = -\frac{8\pi}{k^4} \widehat{\mathrm{K}},$$

and so

$$\widehat{\Phi} = -\frac{8\pi}{k^4}\widehat{\gamma} \quad \rightleftharpoons \quad \widehat{\gamma} = -\frac{k^4}{8\pi}\widehat{\Phi}$$

and

$$\gamma = -\frac{1}{8\pi}\nabla^4\Phi. \tag{5.2}$$

Given a decomposition $r = \Phi + \Theta$, we can then calculate the corresponding screening function γ by simple differentiation of Φ. Conversely, assuming Φ spherically symmetric, we can get Φ for a given γ by solving the biharmonic equation (5.2) in spherical coordinates,

$$\frac{4}{r}\Phi^{(3)}(r) + \Phi^{(4)}(r) = -\frac{1}{8\pi}\gamma(r).$$

5.2   Summary of decompositions

We are now able to complete Tables 5.1 and 5.2, where we list screening functions and corresponding splittings for the Ewald, Hasimoto and Beenakker methods. Some of these results do not appear to be known in the general literature, and have only been previously published in the licentiate thesis [3]. This gives us a comprehensive view of the known Ewald decomposition methods, and also provides us with shortcuts if we want to calculate either decomposition for a given potential. If we, for example, want to calculate the Hasimoto decomposition for a given G, we might be reluctant to carry out the calculation of $(G * \gamma_H)$. If we know K, we can instead get G^R directly by applying K to Θ_H, which in general is a much simpler operation.

Name	Screening function $\gamma(r)$	Fourier screening $\widehat{\gamma}(k)$
Ewald, γ_E	$\alpha e^{-\xi^2 r^2}$	$e^{-k^2/4\xi^2}$
Hasimoto, γ_H	$\alpha e^{-\xi^2 r^2}\left(\frac{5}{2} - \xi^2 r^2\right)$	$e^{-k^2/4\xi^2}\left(1 + \frac{1}{4}\frac{k^2}{\xi^2}\right)$
Beenakker, γ_B	$\alpha e^{-\xi^2 r^2}\left(10 - 11\xi^2 r^2 + 2\xi^4 r^4\right)$	$e^{-k^2/4\xi^2}\left(1 + \frac{1}{4}\frac{k^2}{\xi^2} + \frac{1}{8}\frac{k^4}{\xi^4}\right)$

Table 5.1: Screening functions, $\alpha = \xi^3 \pi^{-3/2}$.

Name	Real space splitting $\Theta(r)$	Fourier space splitting $\widehat{\Phi}(k)$
Ewald, $(\Theta_E, \widehat{\Phi}_E)$	$r\operatorname{erfc}(\xi r) - \frac{r\operatorname{erf}(\xi r)}{2\xi^2 r^2} - \frac{e^{-\xi^2 r^2}}{\sqrt{\pi}\xi}$	$-e^{-k^2/4\xi^2}\frac{8\pi}{k^4}$
Hasimoto, $(\Theta_H, \widehat{\Phi}_H)$	$r\operatorname{erfc}(\xi r) - \frac{e^{-\xi^2 r^2}}{\sqrt{\pi}\xi}$	$-e^{-k^2/4\xi^2}\frac{\pi}{k^4}\left(8 + 2\frac{k^2}{\xi^2}\right)$
Beenakker, $(\Theta_B, \widehat{\Phi}_B)$	$r\operatorname{erfc}(\xi r)$	$-e^{-k^2/4\xi^2}\frac{\pi}{k^4}\left(8 + 2\frac{k^2}{\xi^2} + \frac{k^4}{\xi^4}\right)$

Table 5.2: Splittings, $\Theta(r) + \Phi(r) = r$.

Chapter 6

Quadrature

The term quadrature refers to numerical integration, something which is essential when working with boundary integral methods. We will in this chapter discuss quadrature from a boundary integral perspective, focusing on the special kind of quadrature methods required. The concept of error estimation in the context of quadrature will also be discussed.

6.1 Quadrature rules

A quadrature rule is a method for approximating the definite integral of a function $f(x)$ over some domain Γ,

$$\mathrm{I}[f] = \int_\Gamma f(x)\mathrm{d}x.$$

What we refer to as an n-point quadrature rule is simply a set of n nodes x_i and accompanying weights w_i, which together define the quadrature rule as

$$\mathrm{Q}_n[f] = \sum_{i=1}^n f(x_i)w_i.$$

This is however only an approximation of $\mathrm{I}[f]$, so there is an error in the form of a remainder term,

$$\mathrm{R}_n[f] = \mathrm{I}[f] - \mathrm{Q}_n[f],$$

which goes to zero as $n \to \infty$, assuming f sufficiently well-behaved.

Gauss-Legendre quadrature

A classic example of a quadrature rule is the Gauss-Legendre quadrature rule [1, ch. 25], which by convention is defined for the interval $[-1, 1]$. The qudrature rule

is intimately connected to $P_n(x)$, the Legendre polynomial of order n. The nodes x_i are the roots of P_n,

$$P_n(x_i) = 0, \quad i = 1, \dots, n,$$

and ordered, such that $x_i < x_{i+1}$. The weights are given by

$$w_i = \frac{2}{(1 - x_i^2)P_n'(x_i)^2}.$$

The Gauss-Legendre quadrature rule is extremely efficient for smooth integrands, and a classic result (available in e.g. [18]) is that its remainder satisfies

$$|\,\mathrm{R}_n[f]| \leq \frac{L^{2n+1}(n!)^4}{(2n+1)[(2n)!]^3} \|f^{(2n)}\|_\infty. \tag{6.1}$$

This means that polynomials of degree $2n - 1$ are integrated exactly by an n-point Gauss-Legendre quadrature rule.

6.2   Estimating quadrature errors

Error estimates similar to that in (6.1) exist for most of the classic quadrature methods, such as the trapezoidal [98] and Clenshaw-Curtis [18] methods. However, these methods and their estimates generally assume that the integrand is analytic in a large region around Γ. If the integrand has a singularity close to Γ, then both the methods and their estimates tend to fail, and the estimates are usually the first to do so. Consider the following example from Brass & Petras [18],

$$f(x) = \frac{1}{x^2 + b^2}, \quad b > 0, \quad \Gamma = [-1, 1].$$

Applying (6.1) to this integrand, the bound can simplified to (see Paper III for details)

$$|\,\mathrm{R}_n[f]| \leq \frac{4\pi}{b^2(2b)^{2n}}.$$

This bound diverges for $b < 1/2$, even though f is analytic on Γ and Gauss-Legendre quadrature applied to this integrand exhibits exponential convergence for all $b > 0$ (see example in Figure 6.1). The root cause of this failure is that f has two poles in $\mathbb{C}$, at $z = \pm ib$. The presence of these poles slows down the convergence rate of the quadrature rule, although it still converges. The error estimate, however, is based on the assumption that f is analytic in a large region around Γ, and therefore breaks down when there are poles too close by.

   An alternative way of estimating the quadrature error $\mathrm{R}_n[f]$ is to use the method of contour integrals, as described by Donaldson & Elliott [30]. For that, we let $\mathcal{C}$
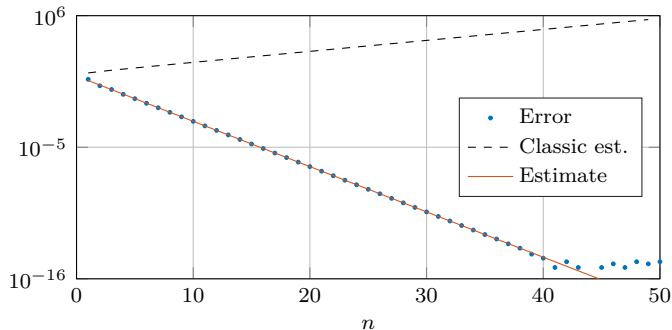
Figure 6.1: Gauss-Legendre rule quadrature error for the function $f(x) = 1/(x^2 + 0.45^2)$ on $[-1, 1]$, plotted versus the number of quadrature nodes. The classic error estimate (6.1) diverges with refinement (since $b > 0.5$), while the improved estimate (6.2) captures the error extremely well.

be a contour in $\mathbb{C}$ that encloses Γ and any poles z_j of f. For a given quadrature rule Q_n there then exists a characteristic error function $k_n(z)$, such that the error R_n is given by the contour integral of $f(z)k_n(z)$ and the residues at the poles,

$$R_n[f] = \frac{1}{2\pi i} \int_{\mathcal{C}} f(z)k_n(z)\mathrm{d}z - \sum_j \mathrm{Res}\left[f(z)k_n(z), z_j\right].$$

For the Gauss-Legendre quadrature rule the error function k_n is not explicitly known, but it can in the limit $n \to \infty$ be shown to satisfy[1] [9, 30]

$$k_n(z) \simeq \frac{2\pi}{(z + \sqrt{z^2 - 1})^{2n+1}}.$$

This turns out to be a good approximation also for small values of n.

In Paper III we use the method of contour integrals for estimating the quadrature error of the Gauss-Legendre rule on $[-1, 1]$ and the trapezoidal rule on the unit circle, when integrating two classes of kernels. The kernels are for $p \in \mathbb{Z}^+$ defined as

$$f_p(z) = \frac{1}{(z - z_0)^p}, \qquad\qquad z, z_0 \in \mathbb{C},$$

$$g_p(x, y) = \frac{1}{((x - x_0)^2 + (y - y_0)^2)^p}, \qquad x, y, x_0, y_0 \in \mathbb{R}.$$

For $p = 1$, these kernels capture the singular behavior of so called double layer potentials in two and three dimensions. For larger p, these kernels model the

---

[1] We here let $a(n) \simeq b(n)$ denote "asymptotically equal to", $\lim_{n\to\infty} \frac{a(n)}{b(n)} = 1$.

integrands encountered when working with the quadrature method that is presented in section 6.5.

Returning to the example function $f(x) = 1/(x^2 + b^2)$, Theorem 2 of Paper III states that the error for this function can be estimated as

$$\mathrm{R}_n[f] \simeq \frac{2\pi b^{-1}}{(b + \sqrt{b^2 + 1})^{2n+1}}.$$

This asymptotic expression is very accurate also for small values of n, as can be seen in Figure 6.1. This particular estimate is however not new, it can also be found in [31]. The contribution of Paper III is mainly that estimates for the model kernels f_p and g_p are derived for arbitrary p.

6.3   Quadrature of boundary integrals

In boundary integral methods, such as the one presented in chapter 3, accurate quadrature is essential for computing the layer potentials involved. These potentials are evaluated through integrals of the form

$$u(\mathbf{x}) = \int_\Gamma G(\mathbf{x}, \mathbf{y})\sigma(\mathbf{y})\mathrm{d}S(\mathbf{y}), \tag{6.2}$$

where σ is a surface density and G is a Green's function that typically is singular along the diagonal $\mathbf{x} = \mathbf{y}$, such that the integrand has a singularity at $\mathbf{x}$ if $\mathbf{x} \in \Gamma$. In this case we say that the integral is singular. The simplest example of such a Green's function is that of the Laplace equation,

$$G(\mathbf{x}, \mathbf{y}) = \frac{1}{|\mathbf{x} - \mathbf{y}|}, \tag{6.3}$$

which inserted into (6.2) gives the Laplace single layer potential. Regular quadrature rules for smooth functions, such as the Gauss-Legendre rule, can be used to evaluate boundary integrals with kernels like (6.3) to high accuracy when $\mathbf{x}$ is sufficiently far away from Γ. When $\mathbf{x}$ is on Γ, however, regular quadrature methods are next to useless due to the singularity in the integrand. If $\mathbf{x}$ is close to Γ, but not actually on it, then we say that the integral is nearly singular, since we are evaluating G close to its singularity. The function $f = (x^2 + b^2)^{-1}$ studied in section 6.2 is for small b an example of this. The nearly singular behavior in boundary integrals causes the error of regular quadrature rules to grow exponentially as $\mathbf{x}$ approaches Γ, effectively creating a problematic region that extends out from Γ.

6.4   Methods for singular and nearly singular quadrature

Largely motivated by the requirements of boundary integral methods, several methods have been proposed for dealing with singular and nearly singular integrals. Most

of the attention seems to have been devoted to the problem of singular integration, as the number of methods available for the problem of nearly singular integration is limited. In many applications, however, both of these problems have to be dealt with. Whenever the geometry includes multiple surfaces that can come arbitrarily close to each other (e.g. particulate flow), or surfaces that can fold back onto themselves (e.g. complex multiphase flow), then accurate nearly singular integration is required for solving the underlying boundary integral equation.

For singular integration, the perhaps most straightforward technique available is that of singularity subtraction [46, 70]. The basic idea is to add and subtract to the integrand a function that kills off the leading order of the singularity, while itself being integrable. A good example of this is the singularity subtraction for the Stokes double layer potential (3.9) that was used in Paper II, which attains third order convergence at virtually no extra cost. Other methods for singular integration include generating specialized quadrature rules for a specific class of singular kernels [20, 19], regularizing the kernel [26, 57, 11], and removing the singularity by a change of variables to a floating partition of unity [22] or a rotated grid [40, 38].

When it comes to nearly singular integration, the methods introduced by Helsing & Ojala [47] allow accurate and efficient evaluation for problems in two dimensions [70, 7]. In three dimensions however, how to best deal with nearly singular integrals on arbitrary surfaces is still something of an open question. For $\mathbf{x}$ moderately close to Γ, acceptable accuracy can be achieved by interpolating the density σ to a finer grid before applying quadrature. This is however not feasible in the limit $\mathbf{x} \to \Gamma$, as the error then grows exponentially, so more specific methods are required. The method by Beale et al. [10, 97] is based on first evaluating a regularized version of the kernel, and then adding a correction to improve accuracy. The method by Ying et al. [107], also used in Quaife & Biros [79], works by interpolating the potential along a line through $\mathbf{x}$ that extends from the surface. Yet another approach is to use a variable change to a floating partition of unity [110] or a rotated grid [Paper II], combined with a sinh transformation [51, 50, 32] that improves accuracy.

The combination of singular and nearly singular integration used in Paper II resulted in a third order overall accuracy, as well as a very costly near singular evaluation. Given that the underlying quadrature rule has spectral accuracy for smooth integrands, third order is clearly suboptimal. Motivated by a wish to improve accuracy and efficiency, much of the work in this thesis has been focused on developing a better quadrature scheme for the problem considered in Paper II. This work, which is presented in Paper IV, is based on the method of quadrature by expansion, introduced in the following section.

6.5 Quadrature by expansion

A fairly recent method for both singular and nearly singular quadrature is the method of quadrature by expansion (QBX), which was proposed by Klöckner et al.
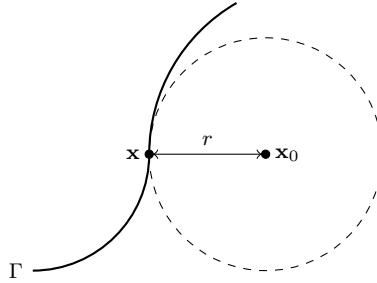
Figure 6.2: QBX geometry. The local expansion formed at $\mathbf{x}_0$ is valid inside the ball of radius r and at $\mathbf{x} \in \Gamma$.

[54], following work by Barnett [8]. The basis of QBX comes from the two following facts regarding layer potentials such as (6.2): (i) They are smooth away from Γ, meaning that they can locally be represented using a Taylor expansion around an expansion center $\mathbf{x}_0$. (ii) They can be accurately computed using regular quadrature if the target point is sufficiently far away from Γ. From these two facts, the method of QBX can for a given quadrature rule and a target point $\mathbf{x}$ on Γ be formulated through the following steps:

1. Pick an expansion center $\mathbf{x}_0$ at a distance r from $\mathbf{x}$ in the normal direction, such that $\mathbf{x}_0$ lies in the quadrature rule's region of high accuracy.

2. Compute the coefficients of a local expansion of the potential around $\mathbf{x}_0$, truncated to some expansion order p.

3. Evaluate the local expansion at $\mathbf{x}$.

The expansion is convergent for all target points $\mathbf{x}_t$ such that $|\mathbf{x}_t - \mathbf{x}_0| \leq r$ [33], as illustrated in Figure 6.2, and therefore also at $\mathbf{x}$. QBX is therefore useful for both singular and nearly singular integrals, as long as the target point is close enough to the expansion center.

For the single layer potential (6.3) a local expansion about a center $\mathbf{x}_0$ can for $|\mathbf{x} - \mathbf{x}_0| < |\mathbf{y} - \mathbf{x}_0|$ be formed using the spherical harmonic addition theorem [41],

$$\frac{1}{|\mathbf{x} - \mathbf{y}|} = \sum_{l=0}^{\infty} \frac{4\pi}{2l+1} \sum_{m=-l}^{l} \frac{|\mathbf{x} - \mathbf{x}_0|^l}{|\mathbf{y} - \mathbf{x}_0|^{l+1}} Y_l^{-m}(\theta_x, \varphi_x) Y_l^m(\theta_y, \varphi_y), \qquad (6.4)$$

where Y_l^m is the spherical harmonic of degree l and order m,

$$Y_l^m(\theta, \varphi) = \sqrt{\frac{2l+1}{4\pi} \frac{(l-|m|)!}{(l+|m|)!}} P_l^{|m|}(\cos\theta) e^{im\varphi}.$$

Here P_l^m is the associated Legendre function, and (θ_x, φ_x) and (θ_y, φ_y) are the spherical coordinates of $\mathbf{x} - \mathbf{x}_0$ and $\mathbf{y} - \mathbf{x}_0$. Inserting (6.4) into (6.2) and rearranging a bit, we get a local expansion of the layer potential,

$$u(\mathbf{x}) = \sum_{l=0}^{\infty} |\mathbf{x} - \mathbf{x}_0|^l \sum_{m=-l}^{l} \alpha_l^m Y_l^{-m}(\theta_x, \varphi_x), \tag{6.5}$$

where α_l^m are the expansion coefficients given by

$$\alpha_l^m = \frac{4\pi}{2l+1} \int_\Gamma |\mathbf{y} - \mathbf{x}_0|^{-l-1} Y_l^m(\theta_y, \varphi_y) \sigma(\mathbf{y}) \mathrm{d}S_{\mathbf{y}}. \tag{6.6}$$

It is worth noting that we have so far made no approximation, (6.5) is an exact expression. What has happened, however, is that we have have changed our singular integral (6.2) into a series of smooth integrals, given by (6.6). We now truncate the expansion at order p and let $\tilde{\alpha}_l^m$ denote the coefficients (6.6) approximated by a regular quadrature rule. The result is the QBX approximation of the layer potential,

$$\tilde{u}(\mathbf{x}) = \sum_{l=0}^{p} |\mathbf{x} - \mathbf{x}_0|^l \sum_{m=-l}^{l} \tilde{\alpha}_l^m Y_l^{-m}(\theta_x, \varphi_x).$$

Error analysis

The error committed when approximating a layer potential using QBX is

$$e(\mathbf{x}) = u(\mathbf{x}) - \tilde{u}(\mathbf{x}) = u(\mathbf{x}) - \sum_{l=0}^{p} |\mathbf{x} - \mathbf{x}_0|^l \sum_{m=-l}^{l} \tilde{\alpha}_l^m Y_l^{-m}(\theta_x, \varphi_x).$$

This error consists of two separate components with different behavior. To see this, we now assume (without loss of generality) that $\mathbf{x}_0 = 0$ and add and subtract the exact coefficients α_l^m from the QBX approximation,

$$e(x) = u(\mathbf{x}) - \sum_{l=0}^{p} |\mathbf{x}|^l \sum_{m=-l}^{l} \alpha_l^m Y_l^{-m}(\theta_x, \varphi_x) + \sum_{l=0}^{p} |\mathbf{x}|^l \sum_{m=-l}^{l} (\alpha_l^m - \tilde{\alpha}_l^m) Y_l^{-m}(\theta_x, \varphi_x).$$

We can write this as

$$e(x) = e_T(x) + e_Q(x),$$

where

$$e_T(x) = \sum_{l=p+1}^{\infty} |\mathbf{x}|^l \sum_{m=-l}^{l} \alpha_l^m Y_l^{-m}(\theta_x, \varphi_x)$$

is the truncation error due to using a finite number of terms in the expansion, and

$$e_Q = \sum_{l=0}^{p} |\mathbf{x}|^l \sum_{m=-l}^{l} (\alpha_l^m - \tilde{\alpha}_l^m) Y_l^{-m}(\theta_x, \varphi_x)$$

is the quadrature error due to evaluating the expansion coefficients using a discrete quadrature rule. The truncation error e_T was analyzed by Epstein et al. [33, Thm 3.1], who showed that there is a constant $M_{\Gamma,\delta}$, $\delta > 0$, such that if σ belongs to the Sobolev space $H^{3+p+\delta}(\Gamma)$, then

$$|e_T| \le M_{p,\delta} r^{p+1} \|\sigma\|_{H^{3+p+\delta}(\Gamma)}.$$

In Paper III of this thesis, we analyze the quadrature error using the method of contour integrals described in section 6.2. One of the main results is that the QBX quadrature error on a square $L \times L$ patch can be shown to behave as

$$|e_Q| \lesssim C \frac{L}{n} \left[1 + \sum_{l=1}^{p} \frac{1}{\sqrt{l}} \left(\frac{4nre}{lL} \right)^l \right] e^{-4nr/L} \|\sigma\|_{L^\infty(\Gamma)}, \tag{6.7}$$

when using the composite Gauss-Legendre quadrature rule with $n \times n$ points. If the ratio nr/L is kept constant under refinement $(n \to 0)$, then

$$e_Q = \mathcal{O}\left(n^{-1}\right) \quad \text{and} \quad e_T = \mathcal{O}\left(n^{-(p+1)}\right),$$

such that the scheme can be viewed as having convergence order $p + 1$, until it hits the lower lever given by the quadrature error. To reduce the error after that (beyond first order), one has to upsample the density σ to a factor κ finer grid before evaluating the coefficient integrals (6.6). This is because because the kernel used to compute the coefficients gets harder to resolve with increasing p, which is also reflected in the quadrature error estimate (6.7).

To summarize QBX, it is a simple scheme that allows evaluation of both singular and nearly singular integrals, with an accuracy that is controlled through the parameters r, p and κ. The nearly singular integration has the benefit of not being target-specific; once all the local expansions are formed it is cheap $(\mathcal{O}\left(p^2\right))$ to evaluate them anywhere inside their ball of convergence. The downside of QBX is that it is expensive to form all the local expansions, especially since it is done using an upsampled grid. A reason for the method being promising is however that the expansions can be formed by linking QBX to a fast multipole method [41] (FMM), which essentially evaluates layer potentials by combining the addition theorem (6.4) with a hierarchical decomposition of the geometry. This would result in an order $\mathcal{O}\left(N\right)$ method, but requires non-trivial modifications to the FMM due to the geometrical requirements of QBX. A general algorithm for the three dimensional problem has not been presented to date, though promising results in two dimensions have recently been presented [82].

QBX for the Stokes double layer potential

In Paper IV of this thesis, we show how QBX can be used to evaluate the double layer potential discussed in chapter 3. This is done for rigid particles of spheroidal shape, for which we develop an acceleration scheme based on precomputations and geometrical considerations. This scheme significantly speeds up the QBX computations, while only requiring a limited amount of memory storage. Together with the fast Ewald method presented in chapter 4 and Paper II, this allows solving Stokes equations for large, periodic particle systems to high accuracy at $M \log M$ complexity, where M is the number of particles.

Chapter 7

Conclusions and future directions

In this thesis we have discussed numerical methods related to two types of fluid flow which are of interest in microfluidics: multiphase flow and viscous flow around rigid particles. The emphasis has however been on methods for viscous flow, which is also reflected in the title of this thesis.

Early work in this thesis was on a method for simulating complex flows involving surfactants and moving contact lines. The method, which is presented in Paper I, is based on an interface tracking method where the interface is decomposed into segments. This provides a natural framework for the treatment of surfactants and contact lines, but is limited to two dimensions. Extending the method to three dimensions is not straightforward, as discussed in [58], which is why this path of development was not continued.

After the work on multiphase flow, the effort of this thesis was directed towards boundary integral methods for Stokes flow. The first project in this direction was on a fast boundary integral method for periodic Stokes flow in three dimensions, applied to sedimentation in particle suspensions. The main results, presented in Paper II, were related to the fast Ewald summation for the Stokes double layer potential.

During the work with the boundary integral method for periodic Stokes flow, the need for a better quadrature method became apparent. The combination of methods used for singular and nearly singular quadrature in Paper II were lacking in both accuracy and efficiency, especially when particles were getting close to each other. To remedy this, work was then started on developing QBX for the Stokes double layer potential and integrating it into the Ewald summation framework. The result, presented in Paper IV, is a fast solver that can deal with singular and nearly singular quadrature in a robust fashion. Along the way, an analysis of the QBX quadrature error resulted in the highly predictive estimates presented in Paper III.

When looking for directions of future development based on the work in this thesis, a couple of options can be seen. First of all it would be natural to apply the framework of Paper IV to the sedimentation problem considered in Paper II,

as the use of QBX removes the problems with nearly singular integration when particles come close to each other. Grid resolution could still be an issue, as seen in Paper IV, but the nearly-touching cases could possibly be ameliorated by coupling the framework to analytic results derived in the lubrication limit [56, 62, 68, 86]. With this in place, a method would be at hand for improving the understanding of sedimentation in suspensions of non-spherical particles. Similarly, the method in Paper IV could in its current state be used for studying the microflow in porous media models involving rigid, non-spherical inclusions. Preliminary results in this direction are included in Paper IV. The acceleration for QBX on spheroidal particles developed in Paper IV could easily be extended to work for any rotationally symmetric shape (with a factor two increased storage), thereby generalizing the scope of the two applications mentioned above.

On the boundary integral side of things, QBX is still a young method with much work to be done, both in analysis and application. In analysis, accurate estimates for the QBX truncation error, similar to those for the quadrature error in Paper III, would be a welcome contribution and is certainly a problem worth devoting some time to. In application, QBX together with an accurate surface representation (such as spherical harmonics) could be used to develop a powerful method for multiphase Stokes flow in three dimensions. QBX precomputations of the type used in Paper IV would then not be possible. Instead, a fast multipole method or a treecode method would be required for computing all the expansions with sufficient efficiency.

Bibliography

[1] M. Abramowitz and I. A. Stegun. *Handbook of Mathematical Functions.* U.S. Govt. Print. Off, Washington, 10 edition, 1972.

[2] S. Adami, X. Hu, and N. Adams. A conservative SPH method for surfactant dynamics. *J. Comput. Phys.*, 229(5):1909–1926, 2010, doi:10.1016/j.jcp.2009.11.015.

[3] L. af Klinteberg. *Computational methods for microfluidics.* Licentiate thesis, KTH Royal Institute of Technology, 2013, http://urn.kb.se/resolve?urn=urn:nbn:se:kth:diva-116384, .

[4] C. K. Aidun and J. R. Clausen. Lattice-Boltzmann Method for Complex Flows. *Annu. Rev. Fluid Mech.*, 42(1):439–472, 2010, doi:10.1146/annurev-fluid-121108-145519.

[5] D. M. Anderson, G. B. McFadden, and A. A. Wheeler. Diffuse-Interface methods in Fluid Mechanics. *Annu. Rev. Fluid Mech.*, 30(1):139–165, 1998, doi:10.1146/annurev.fluid.30.1.139.

[6] K. E. Atkinson. *The numerical solution of integral equations of the second kind.* Cambridge University Press, Cambridge, 1997, ISBN 0-521-58391-8.

[7] A. Barnett, B. Wu, and S. Veerapaneni. Spectrally Accurate Quadratures for Evaluation of Layer Potentials Close to the Boundary for the 2D Stokes and Laplace Equations. *SIAM J. Sci. Comput.*, 37(4):B519–B542, 2015, doi:10.1137/140990826.

[8] A. H. Barnett. Evaluation of Layer Potentials Close to the Boundary for Laplace and Helmholtz Problems on Analytic Planar Domains. *SIAM J. Sci. Comput.*, 36(2):A427–A451, 2014, doi:10.1137/120900253.

[9] W. Barrett. Convergence Properties of Gaussian Quadrature Formulae. *Comput. J.*, 3(4):272–277, 1961, doi:10.1093/comjnl/3.4.272.

[10] J. T. Beale and M.-C. Lai. A Method for Computing Nearly Singular Integrals. *SIAM J. Numer. Anal.*, 38(6):1902–1925, 2001, doi:10.1137/S0036142999362845.

[11]   J. T. Beale, W. Ying, and J. R. Wilson. A Simple Method for Computing Singular or Nearly Singular Integrals on Closed Surfaces. arXiv:1508.00265v1 [math.NA], pages 1–21, 2015.

[12]   C. W. J. Beenakker. Ewald sum of the Rotne–Prager tensor. *J. Chem. Phys.*, 85(3):1581, 1986, doi:10.1063/1.451199.

[13]   T. D. Blake. The physics of moving wetting lines. *J. Colloid. Interf. Sci.*, 299(1):1–13, 2006, doi:10.1016/j.jcis.2006.03.051.

[14]   D. Bonn, J. Eggers, J. Indekeu, J. Meunier, and E. Rolley. Wetting and spreading. *Rev. Mod. Phys.*, 81(2):739–805, 2009, doi:10.1103/RevModPhys.81.739.

[15]   M. Booty and M. Siegel. A hybrid numerical method for interfacial fluid flow with soluble surfactant. *J. Comput. Phys.*, 229(10):3864–3883, 2010, doi:10.1016/j.jcp.2010.01.032.

[16]   J. Brackbill, D. Kothe, and C. Zemach. A continuum method for modeling surface tension. *J. Comput. Phys.*, 100(2):335–354, 1992, doi:10.1016/0021-9991(92)90240-Y.

[17]   J. F. Brady and G. Bossis. Stokesian Dynamics. *Annu. Rev. Fluid Mech.*, 20(1):111–157, 1988, doi:10.1146/annurev.fl.20.010188.000551.

[18]   H. Brass and K. Petras. *Quadrature Theory*, volume 178 of *Mathematical Surveys and Monographs*. American Mathematical Society, Providence, Rhode Island, 2011, ISBN 9780821853610, doi:10.1090/surv/178.

[19]   J. Bremer and Z. Gimbutas. A Nyström method for weakly singular integral operators on surfaces. *J. Comput. Phys.*, 231(14):4885–4903, 2012, doi:10.1016/j.jcp.2012.04.003.

[20]   J. Bremer, Z. Gimbutas, and V. Rokhlin. A Nonlinear Optimization Procedure for Generalized Gaussian Quadratures. *SIAM J. Sci. Comput.*, 32(4):1761–1788, 2010, doi:10.1137/080737046.

[21]   W.-P. Breugem. A second-order accurate immersed boundary method for fully resolved simulations of particle-laden flows. *J. Comput. Phys.*, 231(13):4469–4498, 2012, doi:10.1016/j.jcp.2012.02.026.

[22]   O. P. Bruno and L. a. Kunyansky. A Fast, High-Order Algorithm for the Solution of Surface Scattering Problems: Basic Implementation, Tests, and Applications. *J. Comput. Phys.*, 169(1):80–110, 2001, doi:10.1006/jcph.2001.6714.

[23]   C. Canuto, M. Y. Hussaini, A. Quarteroni, and T. A. Zang. *Spectral Methods*. Scientific Computation. Springer Berlin Heidelberg, Berlin, Heidelberg, 2007, ISBN 978-3-540-30727-3, doi:10.1007/978-3-540-30728-0.

[24] A. Carlson, M. Du-Quang, and G. Amberg. Dissipation in rapid dynamic wetting. *J. Fluid Mech.*, 682:213–240, 2011, doi:10.1017/jfm.2011.211.

[25] S. Chen and G. D. Doolen. Lattice Boltzmann method for fluid flows. *Annu. Rev. Fluid Mech.*, 30(1):329–364, 1998, doi:10.1146/annurev.fluid.30.1.329.

[26] R. Cortez. The Method of Regularized Stokeslets. *SIAM J. Sci. Comput.*, 23(4):1204–1225, 2001, doi:10.1137/S106482750038146X.

[27] R. H. Davis and A. Acrivos. Sedimentation of Noncolloidal Particles at Low Reynolds Numbers. *Annu. Rev. Fluid Mech.*, 17(1):91–118, 1985, doi:10.1146/annurev.fl.17.010185.000515.

[28] P. G. de Gennes. Wetting: statics and dynamics. *Rev. Mod. Phys.*, 57(3):827–863, 1985, doi:10.1103/RevModPhys.57.827.

[29] M. Deserno and C. Holm. How to mesh up Ewald sums. I. A theoretical and numerical comparison of various particle mesh routines. *J. Chem. Phys.*, 109(18):7678, 1998, doi:10.1063/1.477414.

[30] J. D. Donaldson and D. Elliott. A Unified Approach to Quadrature Rules with Asymptotic Estimates of Their Remainders. *SIAM J. Numer. Anal.*, 9(4):573–602, 1972, doi:10.1137/0709051.

[31] D. Elliott, B. M. Johnston, and P. R. Johnston. Clenshaw-Curtis and Gauss-Legendre Quadrature for Certain Boundary Element Integrals. *SIAM J. Sci. Comput.*, 31(1):510–530, 2008, doi:10.1137/07070200X.

[32] D. Elliott and P. R. Johnston. Error analysis for a sinh transformation used in evaluating nearly singular boundary element integrals. *J. Comput. Appl. Math.*, 203(1):103–124, 2007, doi:10.1016/j.cam.2006.03.012.

[33] C. L. Epstein, L. Greengard, and A. Klöckner. On the Convergence of Local Expansions of Layer Potentials. *SIAM J. Numer. Anal.*, 51(5):2660–2679, 2013, doi:10.1137/120902859.

[34] P. P. Ewald. Die Berechnung optischer und elektrostatischer Gitterpotentiale. *Ann. Phys.*, 369(3):253–287, 1921, doi:10.1002/andp.19213690304.

[35] X. Fan, N. Phan-Thien, and R. Zheng. Completed double layer boundary element method for periodic suspensions. *Zeitschrift für Angew. Math. und Phys.*, 49(2):167–193, 1998, doi:10.1007/s000330050214.

[36] S. Ganesan and L. Tobiska. A coupled arbitrary Lagrangian-Eulerian and Lagrangian method for computation of free surface flows with insoluble surfactants. *J. Comput. Phys.*, 228(8):2859–2873, 2009, doi:10.1016/j.jcp.2008.12.035.

[37] S. Ghosh and J. M. Stockie. Numerical Simulations of Particle Sedimentation Using the Immersed Boundary Method. *Commun. Comput. Phys.*, 18(02):380–416, 2015, doi:10.4208/cicp.061113.050115a.

[38] Z. Gimbutas and S. Veerapaneni. A Fast Algorithm for Spherical Grid Rotations and Its Application to Singular Quadrature. *SIAM J. Sci. Comput.*, 35(6):A2738–A2751, 2013, doi:10.1137/120900587.

[39] O. Gonzalez. On Stable, Complete, and Singularity-Free Boundary Integral Formulations of Exterior Stokes Flow. *SIAM J. Appl. Math.*, 69(4):933–958, 2009, doi:10.1137/070698154.

[40] I. Graham and I. Sloan. Fully discrete spectral boundary integral methods for Helmholtz problems on smooth closed surfaces in $\mathbb{R}^3$. *Numer. Math.*, 92(2):289–323, 2002, doi:10.1007/s002110100343.

[41] L. Greengard and V. Rokhlin. A new version of the Fast Multipole Method for the Laplace equation in three dimensions. *Acta Numer.*, 6:229, 1997, doi:10.1017/S0962492900002725.

[42] É. Guazzelli. Sedimentation of small particles: how can such a simple problem be so difficult? *C. R. Mec.*, 334(8-9):539–544, 2006, doi:10.1016/j.crme.2006.07.009.

[43] É. Guazzelli and J. Hinch. Fluctuations and Instability in Sedimentation. *Annu. Rev. Fluid Mech.*, 43(1):97–116, 2011, doi:10.1146/annurev-fluid-122109-160736.

[44] K. Gustavsson and A.-K. Tornberg. Gravity induced sedimentation of slender fibers. *Phys. Fluids*, 21(12):123301, 2009, doi:10.1063/1.3273091.

[45] H. Hasimoto. On the periodic fundamental solutions of the Stokes equations and their application to viscous flow past a cubic array of spheres. *J. Fluid Mech.*, 5(02):317–328, 2006, doi:10.1017/S0022112059000222.

[46] J. Helsing. A higher-order singularity subtraction technique for the discretization of singular integral operators on curved surfaces. arXiv:1301.7276v1 [math.NA], page 7, 2013.

[47] J. Helsing and R. Ojala. On the evaluation of layer potentials close to their sources. *J. Comput. Phys.*, 227(5):2899–2921, 2008, doi:10.1016/j.jcp.2007.11.024.

[48] J. Hernández-Ortiz, J. de Pablo, and M. Graham. Fast Computation of Many-Particle Hydrodynamic and Electrostatic Interactions in a Confined Geometry. *Phys. Rev. Lett.*, 98(14):140602, 2007, doi:10.1103/PhysRevLett.98.140602.

[49] H. Huang, X. Yang, and X.-y. Lu. Sedimentation of an ellipsoidal particle in narrow tubes. *Phys. Fluids*, 26(5):053302, 2014, doi:10.1063/1.4874606.

[50] B. M. Johnston, P. R. Johnston, and D. Elliott. A sinh transformation for evaluating two-dimensional nearly singular boundary element integrals. *Int. J. Numer. Methods Eng.*, 69(7):1460–1479, 2007, doi:10.1002/nme.1816.

[51] P. R. Johnston and D. Elliott. A sinh transformation for evaluating nearly singular boundary element integrals. *Int. J. Numer. Methods Eng.*, 62(4):564–578, 2005, doi:10.1002/nme.1208.

[52] T. Kempe and J. Fröhlich. An improved immersed boundary method with direct forcing for the simulation of particle laden flows. *J. Comput. Phys.*, 231(9):3663–3684, 2012, doi:10.1016/j.jcp.2012.01.021.

[53] S. Khatri and A.-K. Tornberg. A numerical method for two phase flows with insoluble surfactants. *Comput. Fluids*, 49(1):150–165, 2011, doi:10.1016/j.compfluid.2011.05.008.

[54] A. Klöckner, A. Barnett, L. Greengard, and M. O'Neil. Quadrature by expansion: A new method for the evaluation of layer potentials. *J. Comput. Phys.*, 252:332–349, 2013, doi:10.1016/j.jcp.2013.06.027.

[55] J. Kolafa and J. W. Perram. Cutoff Errors in the Ewald Summation Formulae for Point Charge Systems. *Mol. Simul.*, 9(5):351–368, 1992, doi:10.1080/08927029208049126.

[56] a. Lefebvre-Lepot, B. Merlet, and T. N. Nguyen. An accurate method to include lubrication forces in numerical simulations of dense Stokesian suspensions. *J. Fluid Mech.*, 769:369–386, 2015, doi:10.1017/jfm.2015.101.

[57] K. Leiderman, E. L. Bouzarth, R. Cortez, and A. T. Layton. A regularization method for the numerical solution of periodic Stokes flow. *J. Comput. Phys.*, 236:187–202, 2013, doi:10.1016/j.jcp.2012.09.035.

[58] D. Lindbo. *Spectral Accuracy in Fast Ewald Methods and Topics in Fluid Interface Simulation*. PhD thesis, KTH Royal Institute of Technology, 2011, http://urn.kb.se/resolve?urn=urn:nbn:se:kth:diva-48805, .

[59] D. Lindbo and A.-K. Tornberg. Spectrally accurate fast summation for periodic Stokes potentials. *J. Comput. Phys.*, 229(23):8994–9010, 2010, doi:10.1016/j.jcp.2010.08.026.

[60] D. Lindbo and A.-K. Tornberg. Spectral accuracy in fast Ewald-based methods for particle simulations. *J. Comput. Phys.*, 230(24):8744–8761, 2011, doi:10.1016/j.jcp.2011.08.022.

[61] H. Liu and Y. Zhang. Phase-field modeling droplet dynamics with soluble surfactants. *J. Comput. Phys.*, 229(24):9166–9187, 2010, doi:10.1016/j.jcp.2010.08.031.

[62] A. A. Mammoli. The treatment of lubrication forces in boundary integral equations. *Proc. R. Soc. A Math. Phys. Eng. Sci.*, 462(2067):855–881, 2006, doi:10.1098/rspa.2005.1600.

[63] O. Marin. *Boundary integral methods for Stokes flow : Quadrature techniques and fast Ewald methods*. PhD thesis, KTH Royal Institute of Technology, 2012, http://urn.kb.se/resolve?urn=urn:nbn:se:kth:diva-105540, .

[64] S. F. McCormick, editor. *Multigrid Methods*. Society for Industrial and Applied Mathematics, 1987, ISBN 978-1-61197-188-0, doi:10.1137/1.9781611971057.

[65] R. Mittal and G. Iaccarino. Immersed Boundary Methods. *Annu. Rev. Fluid Mech.*, 37(1):239–261, 2005, doi:10.1146/annurev.fluid.37.061903.175743.

[66] M. Muradoglu and S. Tasoglu. A front-tracking method for computational modeling of impact and spreading of viscous droplets on solid walls. *Comput. Fluids*, 39(4):615–625, 2010, doi:10.1016/j.compfluid.2009.10.009.

[67] M. Muradoglu and G. Tryggvason. A front-tracking method for computation of interfacial flows with soluble surfactants. *J. Comput. Phys.*, 227(4):2238–2262, 2008.

[68] S. Nasseri, N. Phan-Thien, and X.-J. Fan. Lubrication approximation in completed double layer boundary element method. *Comput. Mech.*, 26(4):388–397, 2000, doi:10.1007/s004660000188.

[69] P. Nithiarasu. An arbitrary Lagrangian Eulerian (ALE) formulation for free surface flows using the characteristic-based split (CBS) scheme. *Int. J. Numer. Methods Fluids*, 48(12):1415–1428, 2005, doi:10.1002/fld.987.

[70] R. Ojala and A.-K. Tornberg. An accurate integral equation method for simulating multi-phase Stokes flow. *J. Comput. Phys.*, 298:145–160, 2015, doi:10.1016/j.jcp.2015.06.002.

[71] E. Olsson and G. Kreiss. A conservative level set method for two phase flow. *J. Comput. Phys.*, 210(1):225–246, 2005.

[72] Y. Pawar and K. J. Stebe. Marangoni effects on drop deformation in an extensional flow: The role of surfactant physical chemistry. I. Insoluble surfactants. *Phys. Fluids*, 8(7):1738, 1996, doi:10.1063/1.868958.

[73] C. S. Peskin. Numerical-analysis of blood-flow in heart. *J. Comput. Phys.*, 25:220–252, 1977.

[74] C. S. Peskin. The immersed boundary method. *Acta Numer.*, 11(-1):479–517, 2002.

[75] H. Power and G. Miranda. Second Kind Integral Equation Formulation of Stokes' Flows Past a Particle of Arbitrary Shape. *SIAM J. Appl. Math.*, 47(4):689–698, 1987, doi:10.1137/0147047.

[76] C. Pozrikidis. *Boundary Integral and Singularity Methods for Linearized Viscous Flow.* Cambridge University Press, Cambridge, 1992, ISBN 9780511624124, doi:10.1017/CBO9780511624124.

[77] C. Pozrikidis. Computation of periodic Green's functions of Stokes flow. *J. Eng. Math.*, 30(1-2):79–96, 1996, doi:10.1007/BF00118824.

[78] E. M. Purcell. Life at low Reynolds number. *Am. J. Phys.*, 45(1):3, 1977, doi:10.1119/1.10903.

[79] B. Quaife and G. Biros. High-volume fraction simulations of two-dimensional vesicle suspensions. J. Comput. Phys., 274:245–267, 2014, doi:10.1016/j.jcp.2014.06.013.

[80] S. Quan, J. Lou, and D. P. Schmidt. Modeling merging and breakup in the moving mesh interface tracking method for multiphase flow simulations. *J. Comput. Phys.*, 228(7):2660–2675, 2009, doi:10.1016/j.jcp.2008.12.029.

[81] S. Quan and D. P. Schmidt. A moving mesh interface tracking method for 3D incompressible two-phase flows. *J. Comput. Phys.*, 221(2):761–780, 2007, doi:10.1016/j.jcp.2006.06.044.

[82] M. Rachh, A. Klöckner, and M. O'Neil. Fast algorithms for Quadrature by Expansion I: Globally valid expansions. arXiv:1602.05301v1 [math.NA], 2016.

[83] W. Ren and W. E. Boundary conditions for the moving contact line problem. *Phys. Fluids*, 19(2):22101, 2007, doi:10.1063/1.2646754.

[84] Y. Saad and M. H. Schultz. GMRES: A Generalized Minimal Residual Algorithm for Solving Nonsymmetric Linear Systems. *SIAM J. Sci. Stat. Comput.*, 7(3):856–869, 1986, doi:10.1137/0907058.

[85] D. Saintillan, E. Darve, and E. S. G. Shaqfeh. A smooth particle-mesh Ewald algorithm for Stokes suspension simulations: The sedimentation of fibers. *Phys. Fluids*, 17(3):033301, 2005, doi:10.1063/1.1862262.

[86] A. S. Sangani and G. Mo. Inclusion of lubrication forces in dynamic simulations. *Phys. Fluids*, 6(5):1653–1662, 1994, doi:10.1063/1.868228.

[87] R. Scardovelli and S. Zaleski. Direct numerical simulation of free-surface and interfacial flow. *Annu. Rev. Fluid Mech.*, 31:567–603, 1999.

[88] J. A. Sethian and P. Smereka. Level set methods for fluid interfaces. *Annu. Rev. Fluid Mech.*, 35:341–372, 2003, doi:10.1146/annurev.fluid.35.101101.161105.

[89] A. Sierou and J. F. Brady. Accelerated Stokesian Dynamics simulations. *J. Fluid Mech.*, 448:115–146, 2001, doi:10.1017/S0022112001005912.

[90] H. A. Stone. A simple derivation of the time-dependent convective-diffusion equation for surfactant transport along a deforming interface. *Phys. Fluids A Fluid Dyn.*, 2(1):111, 1990, doi:10.1063/1.857686.

[91] H. A. Stone. Dynamics of Drop Deformation and Breakup in Viscous Fluids. *Annu. Rev. Fluid Mech.*, 26(1):65–102, 1994, doi:10.1146/annurev.fl.26.010194.000433.

[92] H. A. Stone, A. D. Stroock, and A. Ajdari. Engineering flows in small devices: Microfluidics toward a lab-on-a-chip. *Annu. Rev. Fluid Mech.*, 36:381–411, 2004, doi:10.1146/annurev.fluid.36.050802.122124.

[93] T. N. Swaminathan, K. Mukundakrishnan, H. H. Hu, and H. U. Howard. Sedimentation of an ellipsoid inside an infinitely long tube at low and intermediate Reynolds numbers. *J. Fluid Mech.*, 551(2006):357–385, 2012, doi:10.1017/S0022112005008402.

[94] P. Tabeling. *Introduction to microfluidics.* Oxford University Press, USA, 2005.

[95] S. Takagi and Y. Matsumoto. Surfactant Effects on Bubble Motion and Bubbly Flows. *Annu. Rev. Fluid Mech.*, 43(1):615–636, 2011, doi:10.1146/annurev-fluid-122109-160756.

[96] K. E. Teigen, P. Song, J. Lowengrub, and A. Voigt. A diffuse-interface method for two-phase flows with soluble surfactants. *J. Comput. Phys.*, 230(2):375–393, 2011, doi:10.1016/j.jcp.2010.09.020.

[97] S. Tlupova and J. T. Beale. Nearly Singular Integrals in 3D Stokes Flow. *Commun. Comput. Phys.*, 14(5):1207–1227, 2013, doi:10.4208/cicp.020812.080213a.

[98] L. N. Trefethen and J. A. C. Weideman. The Exponentially Convergent Trapezoidal Rule. *SIAM Rev.*, 56(3):385–458, 2014, doi:10.1137/130932132.

[99] G. Tryggvason, B. Bunner, A. Esmaeeli, D. Juric, N. Al-Rawahi, W. Tauber, J. Han, S. Nas, and Y. J. Jan. A front-tracking method for the computations of multiphase flow. *J. Comput. Phys.*, 169:708–759, 2001.

[100] M. Uhlmann. An immersed boundary method with direct forcing for the simulation of particulate flows. *J. Comput. Phys.*, 209(2):448–476, 2005, doi:10.1016/j.jcp.2005.03.017.

[101] S. O. Unverdi and G. Tryggvason. A front-tracking method for viscous, incompressible, multi-fluid flows. *J. Comput. Phys.*, 100(1):25–37, 1992, doi:10.1016/0021-9991(92)90307-K.

[102] M. Wang and J. F. Brady. Spectral Ewald Acceleration of Stokesian Dynamics for polydisperse suspensions. *J. Comput. Phys.*, 306:443–477, 2016, doi:10.1016/j.jcp.2015.11.042.

[103] J. F. Wendt, editor. *Computational Fluid Dynamics*. Springer Berlin Heidelberg, Berlin, Heidelberg, 3rd edition, 2009, ISBN 978-3-540-85055-7, doi:10.1007/978-3-540-85056-4.

[104] M. Wörner. Numerical modeling of multiphase flows in microfluidics and micro process engineering: a review of methods and applications. *Microfluid. Nanofluidics*, 12(6):841–886, 2012, doi:10.1007/s10404-012-0940-8.

[105] S. Wrobel. Bubbles, Babies and Biology: The Story of Surfactant. *FASEB J.*, 18(13):1624e–1624e, 2004, doi:10.1096/fj.04-2077bkt.

[106] J.-J. Xu, Y. Yang, and J. Lowengrub. A level-set continuum method for two-phase flows with insoluble surfactant. *J. Comput. Phys.*, 231(17):5897–5909, 2012, doi:10.1016/j.jcp.2012.05.014.

[107] L. Ying, G. Biros, and D. Zorin. A high-order 3D boundary integral equation solver for elliptic PDEs in smooth domains. *J. Comput. Phys.*, 219(1):247–275, 2006, doi:10.1016/j.jcp.2006.03.021.

[108] S. Zahedi, K. Gustavsson, and G. Kreiss. A conservative level set method for contact line dynamics. *J. Comput. Phys.*, 228(17):6361–6375, 2009, doi:10.1016/j.jcp.2009.05.043.

[109] C.-X. Zhao and A. P. Middelberg. Two-phase microfluidic flows. *Chem. Eng. Sci.*, 66(7):1394–1411, 2011, doi:10.1016/j.ces.2010.08.038.

[110] H. Zhao, A. H. Isfahani, L. N. Olson, and J. B. Freund. A spectral boundary integral method for flowing blood cells. *J. Comput. Phys.*, 229(10):3726–3744, 2010, doi:10.1016/j.jcp.2010.01.024.